Revised final ms. May 11, 2008

**[SBI-04 Special Issue of Deep-Sea Research Part II: Topical Studies in Oceanography, 2007 Publication]**

# Sea-ice thickness variability in the Chukchi Sea, spring and summer 2002-2004

Kunio Shirasawa[1*], Hajo Eicken[2], Kazutaka Tateyama[3], Toru Takatsuka[1] and Toshiyuki Kawamura[1]

[1] Institute of Low Temperature Science, Hokkaido University, Kita-19, Nishi-8, Kita-Ku, Sapporo 060-0819 Japan

Phone/FAX: +81-11-706-5425, E-mail: kunio@lowtem.hokudai.ac.jp

[2] Geophysical Institute, University of Alaska Fairbanks, P.O. Box 757320, Fairbanks, AK 99775-7320 USA

Phone: +1-907-474-7280, Fax: +1-907-474-7290, E-mail: hajo.eicken@gi.alaska.edu

[3] Department of Civil Engineering, Kitami Institute of Technology, 165 Koen-cho, Kitami 090-8507 Japan

Phone: +81-157-26-9466, E-mail: tateyaka@mail.kitami-it.ac.jp

**Abstract**

Measurements of sea ice thickness were obtained from drill holes, an ice-based electromagnetic induction instrument (IEM) and a ship-borne electromagnetic induction instrument (SEM) during the early melt season in the southern Chukchi Sea in 2002 and 2004, and in late summer 2003 at the time of minimum ice extent in the northern Chukchi Sea. An ice roughness criterion was applied to distinguish between level and rough or ridged ice. Ice thickness modes in the probability density functions (PDFs) derived from drill-hole and IEM measurements agreed well, with modes at 1.5-1.6 m and 1.8-1.9 m for all data from level ice. The PDFs derived from SEM measurements show that the primary modes are at 0.1 and 1.1 m in 2003 and 0.7 m in 2004. In 2002 and 2004, significant fractions (between one third and one half) of level ice were found to consist of rafted ice segments. Snow depth varied significantly between years, with 2004 data showing more than half the snow cover on level ice to be at or below 0.05 m depth in late spring. Ice growth simulations and examination of ice drift and deformation history indicate that impacts of atmospheric and oceanic warming on level ice thickness in the region over the past few decades are masked to a large extent by variability in snow depth and the contribution of deformation processes. In comparison

with submarine sonar ice thickness data from previous decades, a reduction in ice thickness by about 0.5 to 1 m is in part explained by the replacement of multi-year with first-year ice over the Chukchi and Beaufort shelves.

*Keywords:* Sea ice thickness; Snow depth; Electromagnetic induction instrument; Ice rafting; Ocean heat flux; Chukchi Sea; Beaufort Sea

---

***** Corresponding author: Kunio Shirasawa (Phone/FAX: +81-11-706-5425, E-mail: kunio@lowtem.hokudai.ac.jp)

## 1. Introduction

Fresh and saline water masses that impact the ocean's stratification and thermohaline circulation are partitioned over the Arctic shelves. The shelves also play an important role in inorganic carbon and nutrient cycling, e.g., through fixation and deep-ocean export of carbon as a result of biological activity. With predicted global and regional warming, Arctic shelves will experience longer and more extensive ice-free

conditions, with attendant changes to underwater light climate and wind forcing which in turn will have cascading impacts on Arctic ecosystems (Grebmeier and Harvey, 2005).

Ice formation and decay in the Chukchi and Beaufort Seas and the adjacent sector of the Arctic Ocean, i.e., the study area of the Western Arctic Shelf-Basin Interaction Project (SBI) to which this study contributes, is of importance in or to the Arctic sea ice budget and in or to basin-wide ocean-ice-atmosphere exchange. Sea ice extent has been monitored throughout the Arctic for some decades from space (Gloersen et al., 1992; Comiso, 2002). The decreases observed in the summer minimum ice extent over the past decade or so have been particularly pronounced in the Western Arctic, i.e., the Chukchi and Beaufort Seas north of Alaska (Comiso, 2002; Shimada et al., 2006).

Large-scale surveys by upward looking sonars (ULS) onboard nuclear submarines show a thinning of 42% from a mean draft of 3.1 m in the period 1958-76 to a mean draft of 1.8 m in the 1990s, gathered in various regions of the Arctic Ocean (Rothrock et al., 1999; Tucker et al., 2001). The thinning was 43% in the Chukchi and Beaufort Seas, where mean ice draft decreased from 2.1 m to 1.2 m, while the most pronounced decrease was found in the Eastern Arctic with 1.8 m, or some 55%, from 3.3 m in the earlier period (Rothrock et al., 1999). A more detailed analysis of data collected in the

Western Arctic by Tucker et al. (2001) found additional evidence of substantial thinning in particular in the Beaufort Sea as a result of changes in the ice circulation patterns. The latter were also identified by Rigor and Wallace (2004) as a key contribution to regional ice thinning and retreat in this region.

Further processes responsible for the thinning of sea ice in this area were investigated during the Surface Heat Budget of the Arctic Ocean (SHEBA) study, which included extensive mass-balance measurements at a drifting station in the northern Chukchi Sea (Eicken et al., 2001; Perovich et al., 2003). The SHEBA winter was slightly colder than the long-term average, but the melt season of 1998 was longer, resulting in substantial net thinning of the second-year ice cover over a full year's growth and melt cycle (Perovich et al., 2003). In contrast with earlier studies, such as the 1970s' Arctic Ice Dynamics Joint Experiment, bottom melting both during brief episodes in winter as well as throughout the course of the summer and well into fall was found to contribute substantially to overall ice mass loss, comparable in magnitude to surface ablation (Perovich et al., 2003). Recent evidence from oceanographic surveys and moorings (Shimada et al., 2006; Woodgate et al., 2006) as well as SBI hydrographic measurements (Codispoti et al., 2005), suggest that high ocean heat fluxes to the bottom of the ice cover may contribute to the observed ice thinning. At the same time,

reductions in summer ice concentrations over the past three decades have resulted in a doubling of the amount of solar shortwave radiation that is absorbed in the upper ocean through openings in the pack ice and retreat of the ice edge (Perovich et al., 2007). However, in the absence of dedicated process studies, it is at present far from clear how the relative importance of these processes and their potential interaction impacts the ice mass budget in the study region (see also discussion by Serreze et al., 2007).

In this paper we investigate ice thickness variability in the Chukchi Sea for the spring and summer of 2002, 2003 and 2004, in a region that has experienced some of the most pronounced decadal thinning and summer retreat of sea ice anywhere in the Arctic (Tucker et al., 2001; Shimada et al., 2006). We draw on an ice-based electromagnetic induction instrument (hereafter denoted as IEM) data set, augmented by drill-hole measurements and – in 2003 and 2004 – continuous profiling along the ship's cruise track with a ship–borne electromagnetic induction instrument (hereafter denoted as SEM) system. The aims of this study are two-fold. First, the data compiled are from a region lacking detailed ice thickness surveys, the Chukchi and westernmost Beaufort Shelf, as submarine sonar data have only released for the basin to the North. The question as to whether ice thickness distribution patterns in this region and for these years are comparable to large-scale, decadal patterns is of relevance in the context of the

SBI Program. At the same time, we examine the role of ocean heat flux, snow cover, ice deformation and ice origin on the thickness of ice over the Chukchi and westernmost Beaufort Shelf. While the thickness surveys compiled here are of limited extent as they were constrained by the ship-track, an examination in particular of the level ice portion of the ice thickness distribution can shed some light on the important processes causing sea-ice change in the region. Specifically, we hypothesize that in addition to the factors discussed above, interannual and regional variability in level ice thickness over the shelf is significantly impacted by snow cover variations and "hidden" deformation of level ice through rafting processes.

## 2. Data Acquisition and Analysis

### 2.1. Study Area and Measurements

Ice thickness measurements were carried out during the SBI spring process cruises into the southern Chukchi Sea in 2002 and 2004 with the *US Coast Guard Cutter Healy* (Grebmeier and Harvey, 2005), and during the Second Chinese National Arctic Expedition (CHINARE-2003) in the northern Chukchi Sea in late summer in 2003 with

the Chinese Polar Research Institute's *R/V Xuelong* (Shirasawa et al., 2006). All expeditions took place from mid-May to early September (Table 1), extending from just prior to the onset of melt to fall freeze-up. Locations of the measurements on ice floes are given in Table 1 and the cruise tracks are shown in Figs. 1(a)-1(c). In 2002 and 2004, the measurements were part of the SBI field experiments in the southern Chukchi and western Beaufort Sea, whereas in 2003 the IEM and SEM ice thickness measurements were made in the northern Chukchi Sea as part of the CHINARE-2003 expedition into the summer Chukchi and Beaufort Seas.

During the SBI cruises, a sea-ice coring program was carried out that included measurements of ice properties to aid studies of ice-associated biological production and sediment-transport by sea ice (Eicken et al., 2005; Gradinger, this volume). At each measurement site representative ice cores were drilled in close proximity to the thickness profile. Immediately after drilling, temperatures were measured in small drill-holes in the core at 5-10 cm intervals by inserting a thermistor probe. Cores were then sectioned into 5-10 cm pieces and transferred to the laboratory for a range of measurements, including ice bulk salinity (with a YSI 85 conductivity probe, measurement error <0.02 or <1 % of the bulk salinity), brine volume fraction and ice microstructure. Further, snow density and temperature were measured at 1-3 cm vertical

intervals, and the snow salinity was determined on melted samples as described above. At the drill site, under-ice hydrographic measurements were carried out with the YSI 85 conductivity probe in 2002 or the SBE-19 Conductivity-Temperature-Depth probe (CTD) in 2003 and 2004. During the CHINARE-2003 cruise, a sea-ice coring program and under-ice hydrographic measurements were also carried out in the same fashion as during the SBI cruises.

In addition to the on-ice research program, observations of ice conditions were made at 2 hour intervals for 10 minutes from the ship's bridge by a team of four observers. Observations covered a corridor of 1 km width to either side of the ship's track and comprised determination of prevailing ice types, ice thickness, snow depth, and distribution of open water. Digital photographs of ice conditions to port and starboard and photographs of ice features (including ice stratigraphy as exposed in broken floes tilted upright along the vessel's hull) complemented the observations. Data and photographs of these observations are available on-line through the SBI Data Catalog (www.eol.ucar.edu/projects/sbi/).

IEM ice thickness measurements were carried out during the SBI and CHINARE cruises by towing or carrying an EM instrument along profiles of typically several hundred meters length with measurement intervals of 1 to 5 m (Table 1). At each of

these measurement points, snow depth (and if present, melt pond depth) was also determined. Profiles were located in ice representative of the overall ice conditions (based on the ship-based observation program) and the profile was situated so as to sample a representative area, including ridges and deformed ice. At a few points at each station, ice thickness and freeboard were determined in a 5-cm drill hole. During both SBI cruises (2002 and 2004) the entire width of the seasonal ice was traversed by the vessel with a few sampling sites located in the multi-year pack to the North (Fig. 1, Table 1). EM conductivity calibration data was obtained from ice and water samples, as described for ice cores before.

### 2.2. Methodology of EM Ice Thickness Measurements

Measurements of sea ice thickness with an ice-based EM (IEM) (e.g., Haas et al., 1997; Eicken et al., 2001; Haas and Eicken, 2001;Tateyama et al., 2004), ship-borne EM (SEM) (e.g., Haas, 1998; Worby et al., 1999; Uto et al., 2002; Reid et al., 2003; Shirasawa et al., 2006) and air-borne EM (e.g., Kovacs et al., 1987; Kovacs et al., 1995) have been made widely in the Arctic and Antarctic sea-ice zone.In seasonally ice-covered waters, SEM measurements of sea ice thickness have been conducted in the

southernmost part of the Sea of Okhotsk, in highly deformed ice of the coastal region (Uto et al., 1999; Tateyama et al., 2006; Uto et al., 2006).

All IEM measurements carried out for this study were made with a single-frequency EM sensor with an internal battery pack (EM–31/Mk2, Geonics Ltd., Canada). All SEM measurements utilized in the present study were made by combining an EM-31/ICE (Geonics Ltd., Canada) with an external battery, with a laser altimeter onboard an icebreaker (Fig. 2). The laser altimeter (LD90−3100HS, Riegl, Austria) detects the distance from the sensor to the surface of snow or ice. The EM-31 instrument generates an electromagnetic field (9.8 kHz) in a transmitter coil (Tx, Fig. 2) and detects the strength of the field induced in the half-space underneath the instrument through a receiver coil (Rx). The primary magnetic field $H_p$ generated by the Tx induces eddy currents in the underlying seawater. These currents generate a secondary magnetic field $H_s$, which is sensed along with $H_p$ by Rx. The EM-31 instrument automatically transforms the measured quadrature response of $H_s$ to the apparent conductivity $\sigma_a$ in mS/m (McNeill, 1980). The $\sigma_a$ is defined as

$$\sigma_a = \frac{4}{\omega \mu_0 r^2} Q\left(\frac{H_s}{H_p}\right) \qquad (1)$$

where $\mu_0$, $\omega$, $r$, and $Q(H_s/H_p)$ denote the magnetic permeability of free space ($4\pi\times10^{-7}$ H/m), angular frequency ($\omega=2\pi f$), transmitter–receiver coil separation (3.66 m) and the quadrature component of the ratio of $H_s$ to $H_p$ at Rx, respectively. The strength of the induced field is inversely proportional to the distance of the interface between the low-conductivity ice and the high-conductivity seawater. Based on empirical and modeling studies we can derive an estimate of ice thickness from those measurements. The salinity of the ice is of little consequence in this regard because of its strong contrast (three orders of magnitude) with seawater conductivity, however, in the 3-layer modeling described below we have integrated ice conductivities based on field measurements during the cruise.

Since the difference in the conductivity between snow and ice is very small, the EM instrument cannot distinguish between the two. Therefore, we discuss the relationship between $\sigma_a$ derived from EM measurements and the observed total thickness of snow and ice ($Z_S + Z_I$), where $Z_S$ is the snow depth and $Z_I$ is the ice thickness. The total thickness can be calculated by subtracting the distance between the EM sensor and the snow/ice surface ($Z_L$), either measured as the hip height of a person carrying the EM on the ice floe during the CHINARE-2003 and as the height of the EM placed on the sledge towed across the ice during the SBI-02/-04 for IEM measurements,

or measured by a laser altimeter as the distance between the EM sensor and the seawater surface ($Z_E$) for SEM measurements. During CHINARE spacing of snow depth measurements was mostly larger than 10 m and individual ice thickness measurements were derived by subtracting the mean snow depth along the profile from individual total thickness data points.

The $\sigma_a$ value can be measured in either a horizontal coplanar (HCP) mode or a vertical coplanar (VCP) mode. In the present study we used the former mode for IEM measurements in 2002 and 2004 and the latter for IEM measurements in 2003 and all SEM measurements. According to Reid and Vrbancich (2004), the footprint size for the VCP and HCP geometry is 1.4-1.5 and 3.7 times larger than the $Z_E$, respectively. For SEM measurements during the CHINARE-2003 and SBI-04 cruises, the EM instrument was operated in VCP mode and placed 5.6-6.0 m away from the ship's hull at an operating height of 4 m (Fig. 2) to minimize effects of the ship's hull on the EM fields (Shirasawa et al., 2006).

A method to calculate the total thickness of snow and ice from the apparent conductivity $\sigma_a$ by using a 1-D multi-layer model was proposed by Haas et al. (1997) and Haas (1998). In the present study, we used the program PCLOOP, developed by Geonics Ltd. (McNeill, 1980), to calculate $\sigma_a$ based on a 1-D multi-layer model, which

consists of three layers (snow, ice and seawater). The instrument height ($Z_L$) was also included in this model. For the IEM measurements (HCP mode), the total thickness ($Z_{S+I}$) was converted by the following equation (Eicken et al., 2001):

$$Z_{S+I} = 8.167 - \ln(\sigma_a - 57.35)/0.8406 - Z_L \quad (2)$$

where $Z_L$ is the instrument height between the EM sensor placed on the sledge and the snow surface.

To invert VCP mode measurements, a model proposed by Tateyama et al. (2006) was used:

$$Z_{S+I} = 11.22 - \ln(\sigma_a - 14.47)/0.6049 + dZ_E \quad (3)$$

where $dZ_E$ is the offset of the thickness, which can be expressed as a constant hip height for IEM measurements in 2003. For SEM measurements, $dZ_E$ was determined empirically from the data obtained during SEM measurements in 2003 by the *Xuelong* and in 2004 by the *Healy* (Tateyama et al., 2006).

A comparison between observed the apparent conductivities (derived from eq.

(1)) and measured drill-hole ice thicknesses is shown in Fig. 3(a). The solid line is derived from eq. (2) for the HCP mode, and the dashed line is derived from eq. (3) for the VCP mode. For thicknesses less than 1-2 m, some EM-based ice thicknesses are estimated to be larger than observed drill-hole thicknesses. While the thickness derived from the standardized $\sigma_a$-$Z_{S+I}$ transformation equation, eq. (3), based on a 1-D three-layer model consisting of snow, ice and seawater layers, considers the effects of seawater-filled gaps in deformed ice, a surface slush layer and the instrument footprint, the difference between drill-hole and EM measurements depends strongly on ice roughness relative to footprint size. Previously, Tateyama et al. (2006) found higher deviations (average of >12%) in highly deformed ice. Reid et al. (2006) examined the problem in more detail and concluded that differences in footprint size strongly impact comparisons such as shown in Fig. 3. Unless data are averaged over longer distances, which reduce discrepancies in footprint size, comparisons between the two measurement approaches are more compatible in level ice. In this study, EM-derived ice thicknesses were further separated into level and deformed ice, defined as exhibiting a variance below or above a threshold for the set of ice thickness measurements centered on a specific point and with its nearest neighbors to either side. Based on a study by Tin and Jeffries (2003), for IEM measurements a combination of that threshold, set as 9%

for the gradient, and of two neighboring points to either side, set as 5 m, was considered. The relation of IEM total thickness to drill-hole total thickness for level and deformed ice, determined in this fashion, is shown, as both thicknesses agree well in the range up to 3 m (Fig. 3(b)). It, however, appears that differences between the EM- and drill-hole measurements are higher in deformed ice more than 4 m thick. Since those deviations are likely a result of the limited lateral resolution of the EM instrument, further study of this problem requires a 3-D multi-layer model approach. By averaging over long profiles and by distinguishing between level and deformed ice, we are minimizing the error resulting from this effect.

## 3. Results

### 3.1. Ice Cores and Under-ice Hydrography

Results of ice core analysis showing a representative sample obtained during the 2002 cruise from a floe representative of ice in the area (km-sized level ice floes separated by zones of ice rubble) are presented in Fig. 4. Ice salinity increases with depth from 3.1 psu at the top to 6.3 psu at the 0.4 m depth and reaches 8 psu at the bottom of the 0.9-m-thick ice core (Fig. 4(a)), indicating that surface meltwater flushing has not set in yet (only during the last few days of sampling in 2002 was surface melt

affecting the underlying ice). With $\delta^{18}$O between 0 and –5 ‰, the impact of meteoric water present at the time of freeze-up is apparent. The salinity and stable isotope profile indicate that this is a rafted piece of ice, possibly with some entrainment of snow at the 0.3 m depth level.

As representative of cores taken in 2003, the sample shown in Fig. 4(b) shows signs of surface melt and meltwater flushing. While the bulk of the ice is clearly of marine origin based on stable isotope data, the under-ice water does indicate meltwater entrainment with a salinity of 12.5 psu and $\delta^{18}$O of -3.1 ‰. Overall, $\delta^{18}$O values for sea ice and under-ice seawater in the 2003 study area are similar to those of the average Arctic Ocean surface $\delta^{18}$O field, as reconstructed from $\delta^{18}$O profiles from sea ice cores coupled with back trajectories of ice drift and a simple ice growth model (Pfirman et al., 2004). Cores sampled in 2004 (see representative core in Fig. 4(c)) exhibited some signs of brine drainage and meltwater flushing, in particular during the second half of the cruise.

A layer of warmer and fresher water was found just below the ice in all three years, as indicated in the soundings shown for mid-May 2002, late August 2003 and mid-June 2004 (Fig. 4(d)-(f)). Based on a study tracking the fate of snow and ice meltwater after the onset of ablation (Eicken et al., 2002), it appears likely that this layer

is largely derived from surface and bottom ice melt and that parts of this water may have persisted into the freeze-up season.

### 3.2. Ice Stratigraphy from Ship-board Observations

Photographs of ice-floe cross-sections taken during standard ship-based ice observations allowed us to assess the fraction of deformed (in particular rafted) level ice. Out of a total of 236 photographs 112 showed proper cross-sections (rather than the surface or some other aspect of ice passing by the hull of the ship without being turned on its side) to be analyzed for any evidence of ice deformation, either in the form of large (>0.2 m) ice fragments embedded in a matrix of frazil and congelation ice or evidence of ice rafting. Fig. 5 shows an example of a level ice floe of roughly 1.5 m thickness turned on its side along the ship's hull, showing evidence of multiple rafting in its upper half and embedding of fragments and rafts of ice among a matrix of frazil (containing suspended sediment particles as well, Eicken et al., 2005). Both the photographs and the accompanying ice observations allowed us to distinguish between undeformed (though often naturally banded), congelation-growth ice (such as that constituting the individual layers that make up each raft shown in Fig. 5) and deformed

ice. Mostly, the floe cross-sections examined are representative of overall level ice in the area, though there is some bias towards thinner ice in areas of thick ice as the ship's track was dictated by the search for level ice or open water for easy navigation.

A summary of these observations is provided in Table 2, giving the fraction of all observations with evidence of deformation in level ice. While no attempt has been made to account for the volume fraction of deformed ice within each individual floe, in most instances at least half the floe thickness contained deformed ice, quite often much more, such as shown in Fig. 5. As the cruise in 2002 focused on entrainment of sediments into sea ice (Eicken et al., 2005), the imagery collected may exhibit a bias towards floes containing sediments (i.e., with additional sediment-laden ice photos taken outside of the proper 10-minute observation interval, or with the sediment-laden ice photographed if two or more ice types were present), which in turn may be associated with a bias towards deformed ice. In 2004 this was not the case. Taking these circumstances into consideration, it is nevertheless apparent that a significant portion of the level ice (between one third and up to one half) is in fact composed of ice resulting from deformation processes, mostly rafting.

### 3.3. Ice-based EM (IEM) Ice and Snow Thickness Measurements

The results of all ice-based EM (IEM) measurements, including locations and summary statistics, are listed in Table 1, with representative ice floe transects for all three years shown in Fig. 6. As discussed in Section 2.2, deviations between drill-hole and IEM measurements in rough ice are largely due to differences in footprint size and 3-dimensional thickness variability not accounted for by the one-dimensional EM data processing scheme. The thickness measurements as well as ship-based ice observations indicate that ice floes are mostly of a composite nature with level sections (including frozen leads) alternating with ridged or rubbled ice. Both, ice observations from the ship's bridge and ice core analysis (see previous section) indicate that the transition between first-year ice in the seasonally ice-free sectors of the Chukchi and Beaufort Seas and the multiyear ice pack was located near the northernmost end of the N-S transects. At the northernmost stations (such as Ice St. 020523 in Table 1), multiyear ice floes of around 2 m or less in thickness were typically separated by a combination of deformed and thin (<1 m) level first-year ice.

Ice thickness probability density functions (PDFs) for 0.1 m bin size were computed from IEM measurements for all three years (Fig. 7). The PDFs derived from drill holes compare well with those from IEM measurements for level ice with the most

prominent modes at 1.4 and 1.8 m thickness (see also Fig. 3(b)). For deformed ice several modes are apparent, however, none of these is a distinct primary mode associated with a particular ice class; rather, ice thickness is distributed across a broad range (Fig. 7). In 2002, three thickness modes at 0.5, 1.1 and 1.5 m prevailed in the level first-year ice of the Southern Chukchi Sea (Fig. 8). The primary ice thickness mode extends from 1.4 to 1.6 m. Thicker level ice includes two transects that in part traversed multiyear ice at two sites (Ice St. 020521 and 020523 in Table 1). One of these floes (Ice St. 020521) contained segments (few hundred meters wide) of thick (2 to 4 m) multiyear ice with a pronounced, rolling topography. The salinity profile and stratigraphy of the ice core obtained at this location indicate that the ice is at least third-year ice. Snow depths on this old ice averaged 0.21 $\pm$ 0.14 m. The other sampling site (Ice St. 020523) consisted of a large floe of mostly level multiyear ice, between 1.6 and 1.9 m thick, interspersed with first-year ice pans and ridges. The thin ice represented in the mode extending from 0.4 to 0.7 m was sampled in the southernmost Chukchi Sea below 70˚N (Fig. 1(a)).

In 2004, ice thicknesses in roughly the same sector of the Chukchi Sea exhibited the mode at 1.9 m (Fig. 8). In late summer of 2003, in the northern Chukchi Sea, the primary ice thickness mode was at 1.5 m (Fig. 8), representative of late season

second-year or very thick first-year level ice.

Fig. 9 shows the PDF for snow depth on level ice for the 2002 and 2004 cruises into the southern Chukchi Sea. Since the latter part of the cruises took place after surface melt had set in, all data collected after the first day on which surface melting temperatures were observed were excluded from the analysis (prior to 5 June 2002 and prior to 31 May 31 2004). In 2004, the snow depth PDF exhibits a distinct mode at 0.02 to 0.04 m, while in 2002, snow depth distribution is somewhat broader, lacking a distinct primary mode. Snow and ice mass balance measurements at Barrow (Eicken et al., 2005, see also www.gi.alaska.edu/snowice/sea-lake-ice/Data/sea_ice_data.html) indicate a mean snow depth on landfast ice of 0.15 ± 0.03 m in 2002 and anomalously low snow depths of 0.02 ± 0.01 m in 2004.

### 3.4. Ship-borne EM (SEM) Thickness Measurements

The total ice thickness along the *R/V Xuelong* cruise track obtained by SEM measurements in August/September of 2003 (Shirasawa et al., 2006) is shown as a function of time starting from 24 August 2003, in Fig. 10(a). The ice concentration along the ship cruise track, as estimated from the open water area which was detected

by the laser distance meter at 1-second intervals over the 1-min measurement period, is also shown. SEM measurements were mainly carried out along the two hydrographic survey lines, i.e., parallel to the ice edge along a latitudinal line and along a meridional line from the ice edge up to 81$^{o}$N (Fig. 1(b) and (e)). SEM measurements were only conducted in the regions farther from the ice edge, where compact ice fields mainly filled with deformed ice floes were dominant. During the period from 24 to 26 August, the ship proceeded towards the north and reached the northernmost site of the CHINARE-2003 field campaign at approximately 81˚N, where sea ice with thicknesses around 0.3- m-, 1.5- to 2.0- m- and 4 -m was dominant. The ship headed, thereafter, towards the south through loose ice fields from 27 August onwards. After ramming into a thicker multi-year ice field, the ship anchored at a large ice floe for a long-term experiment until 4 September. After that, the vessel sailed along the ice edge (Fig. 1(b) and 1(e)), where ice floes less than 1.5 m thick were dominant in open pack ice. As evident from Fig. 1(e), ice had retreated substantially from the southern Chukchi Sea, while the northern Chukchi and even the central Arctic Ocean were also displaying much less concentrated ice cover at the beginning of September in 2003.

The PDF of total thickness (0.1 m bin size) derived from SEM measurements of 2003 is shown in Fig. 11. The primary thickness modes were at 1.1 m, most likely

corresponding to first-year level ice, and at a thinner thickness (0.1 m), indicative of thin, rotting ice late in the season.

The total thickness and ice concentration derived from SEM measurements along the *Healy* cruise track in May/June of 2004 is shown in the same manner as those of the *Xuelong*, in Fig. 10(b). SEM measurements were carried out mainly along the ice edge in the southern Chukchi Sea (Fig. 1(c) and (f)), where ice concentrations were lower than in the northern Chukchi, Siberian and central Arctic Seas with a densely packed sea ice cover, as seen in Fig. 1(f). The southern half of the study region, extending down to 70$^{o}$N in the southern Chukchi Sea, exhibited a less concentrated ice cover, in contrast with the closed pack in the northern half of the study region, extending up to 73$^{o}$N (Fig. 10(b)). Compared to 2002, sea ice extent in the southern Chukchi Sea at the beginning of June was larger in 2004 (Fig. 1).

The PDFs derived from SEM measurements in 2004, shown in Fig. 11, exhibit a primary thickness mode at 0.7 m for first-year level ice.

## 4. Discussion

As discussed in the introduction, the principal aim of this study is to consider

the thickness of sea ice in the SBI study area in the context of atmosphere and ocean variability and change. While our conclusions are constrained by the somewhat limited scope of the data set collected during the three ship cruises, the role and relative importance of a number of key factors implicated in the recent sea-ice thinning and retreat observed in the East Siberian and western North American sector of the Arctic can nevertheless be evaluated. Specifically, after a discussion of potential errors and limitations of the data set, we will consider the age, circulation and deformation history of the ice, its growth history, and the impact of atmospheric and oceanic heat transfer on ice growth, as well as the role of snow-cover variations.

### 4.1. Discussion of Sampling and Random Errors

A number of studies have examined the accuracy of EM induction measurements of ice thickness. Detailed 1- and 2-D surveys in the field (Kovacs et al., 1987; Haas and Eicken, 2001) have established that for solid ice, lacking any internal seawater-filled cavities, measurement accuracy is generally better than 0.05-0.1 m at thicknesses below 2.5 m. This error increases to values of 0.1 to 0.15 m in the presence of surface or under-ice meltwater layers, assuming that these are not accounted for in

the conductivity model or inversion equation (Eicken et al., 2001). The problem in comparing ice thickness measurements from drill holes with EM data is the vastly different footprint size (<0.1 m as compared to several meters) which can result in substantial discrepancies in particular in ridged or rough ice, with the latter requiring a more sophisticated conductivity inversion approach (Kovacs et al., 1995; Reid et al., 2006). Much of the scatter apparent in Fig. 3(a) is explained by such discrepancies. Here, we have distinguished between level ice and ridged or rough ice to address this problem, with accuracies for level ice data estimated at better than 0.1 m at thicknesses below 2.5 m and those for ridged ice ranging between 0.1 and 0.5 m depending on ice thickness and roughness. Note that these errors include the errors inherent in the apparent conductivity measurement, based on sensitivities derived from the transformation equations shown in Fig. 3(a).

Distinguishing between level and ridged or rough ice significantly improves the sampling statistics and reduces random errors, since the inherent variability in level ice thickness is substantially smaller both at the floe- as well as the regional scale. Standard deviations for level ice are lower than those of ridged ice by a factor of roughly 2 (Table 1), with disproportionately much larger sample sizes for level ice. Applying t-tests to both the 2002 and 2004 level ice data sets indicates that the two samples are in fact from

populations with different mean values (significant at the 0.01-level). At the same time, differences between the level thin- and thick-ice modes are significant as well. While a detailed investigation of sampling statistics is beyond the scope of this paper, we note that the typical profile length is of the same order of magnitude as the largest autocorrelation lengths reported in the Arctic (Rothrock and Thorndike, 1980) and one to two orders of magnitude larger than autocorrelation lengths reported for rough ice (Lange and Eicken, 1991). Hence, the measurements made at different stations (and those of long profiles sampling different segments of composite floes) constitute independent samples of the regional distribution of level ice.

### 4.2. Ice Circulation and Drift History of the Ice Cover in the Study Area

In order to interpret observed ice thickness patterns in a broader regional and interannual context, the origin and drift history of the ice cover needs to be taken into consideration. For all three years, a number of buoys deployed as part of the International Arctic Buoy Program (IABP) pass through the study region roughly at the same time as sampling took place (Fig. 12). For both years, 2002 and 2004, ice drift followed the circulation pattern characteristic of the Beaufort Gyre, with ice advected

from the northeastern Beaufort Sea and Eastern Canadian Basin over the course of the previous fall and winter, drifting roughly parallel to the east-west orientation of the northern Alaska coastline (Fig. 12(a, c)). Ice velocities were higher than long-term averages and conformed with more rapid ice motion ascribed to surface circulation patterns associated with low atmospheric pressure over the central Arctic (high Arctic Oscillation, AO, Index) by Rigor et al. (2002) in their analysis of Arctic buoy drift. While rapid northward export as reported by Tucker et al. (2001) for the 1990s was not observed for the ice fields sampled in this study, the buoy data suggested reduced residence times in the Beaufort Gyre as compared to climatology. In 2003 (Fig. 12(b)), circulation patterns of the sampled ice were more variable, which is attributed in large part to the location of the sampling sites near the center of the Beaufort Gyre where velocities are slower and trajectories more erratic (Rigor et al., 2002).

An examination of the location of the summer minimum ice edge during the summers preceding the ship cruises in 2002 and 2004 indicates that most of the area sampled lay well outside of the perennial ice edge and is hence first-year ice in origin. This finding agrees well with the observations of a predominance of first-year ice obtained from ice-core measurements and observations of ice morphology, both of which suggest that multiyear ice was limited to the northernmost edge of the study area

in 2002 and 2004. The 2003 sampling, however, took place mostly in multiyear ice based on examination of trajectories and remote sensing data. For the 2003 study region, submarine sonar data from the 1980s and 1990s have been released by the National Snow and Ice Data Center (NSIDC) and provide a reference to the data reported here (see map in Fig. 13, PDFs of ice thickness in Fig. 14). The late-summer submarine data for 1989 and 1992 exhibit comparable modes attributable to level ice with no significant differences in thickness (i.e., modes <2 m), whereas the late-summer data from 1988 correspond to substantially thicker ice with modes >3 m.

The 2002 and 2004 level-ice thickness data display significantly smaller modes than the submarine data collected in late spring, which we attribute mostly to the fact that the sonar data have been obtained from multiyear as opposed to first-year ice. In fact, if one assumes that with prevailing ice circulation patterns in the 1980s (Tucker et al., 2001; Rigor et al., 2002) and less extensive summer ice retreat (Shimada et al., 2006), the ice in the study area in the 1980's and 1990's was mostly composed of multiyear ice, then a significant portion of the ice thinning over the Beaufort and Chukchi shelves would be attributable to replacement of multiyear by first-year ice, along with reduced residence times of ice drifting through the region. This is confirmed by the ship-based observations and analysis of QuikSCAT radar scatterometer data,

obtained as gridded backscatter coefficient maps from the French European Remote Sensing Satellite Processing and Archiving Facility (CERSAT, www.ifremer.fr/cersat/en/data/download/gridded/psiqscat.htm) (Figs. 1(g)-(i)). Ezraty and Cavanie (1999a and b) have demonstrated that radar backscatter coefficients $\sigma^0$ are highly effective in distinguishing between first-year and multiyear ice, with first-year ice characterized by $\sigma^0 \leq 0.08$ at the Ku-band frequencies relevant to QuikSCAT. As shown in Figs. 1(g)-(i), the transition between first- and multiyear ice coincides with or is well north of the northernmost extent of the data set collected here. This finding of reduced ice age is in line with suggestions by Tucker et al. (2001), Rigor and Wallace (2004) and others who examined ice circulation patterns in the region.

Analysis of ice drift history of the ice in the southernmost Chukchi Sea (sampled at a few sites in 2002 and at one site in 2004), which exhibited mean and modal thicknesses well below 1.5 m (in some cases less than 1 m, see Table 1 and Fig. 7), indicates a much younger in age of at most 3-4 months at the time of sampling. This has been discussed in depth by Eicken et al. (2005) relying on observed and simulated backtrajectories in their analysis of sediment transport by sea ice.

### 4.3. Impact of Air Temperature, Snow Cover and Ocean Heat Flux on Ice Growth

**History**

The extent to which interannual variability and longer-term change may have impacted observed level ice thicknesses and ice growth was assessed with a simple freezing-degree day analytical ice-growth model (Maykut, 1986; Eicken, 2003). The model was forced with mean daily air temperatures measured at the Barrow National Weather Service station in 2002, 2003 and 2004. Climate normals (1971-2000) were also used in the simulations to determine deviation from climatology. The results of these simulations are shown in Fig. 15 for two age classes of sea ice commensurate with the analysis of ice origin and drift history (see previous section), i.e., ice formed on 1 October and 1 February of each ice season. Simulations were completed for three different snow depths of 0, 0.1 and 0.25 m (assumed constant as constrained by the analytical model, cf. Maykut, 1986). Interannual variations in snow-free ice are comparatively small, with the largest deviations between climatology and individual years, the former larger by 0.05 m (2002), 0.25 m (2003) and 0.08 m (2004) at the end of the ice-growth season on 31 May. As to be expected, the corresponding differences for ice that formed on 1 February are smaller, with a maximum deviation of 0.09 m between climatology and ice grown in 2003. The insulation provided by a thicker snow

cover reduces interannual variations, with a maximum of 0.16 m thickness difference between climatology and ice formed on 1 October 2002 with a snow cover of 0.25 m depth.

The importance of snow accumulation on sea ice in controlling ice growth through bottom freezing and its potential impact on interannual variability in ice thickness is evident from simulations constrained by observed snow depths and ice formation dates obtained in the landfast ice of Barrow, Alaska in the years 2002 and 2004 (Fig. 15). In 2004, snow depths were very low (0.03±0.01 m) due to late ice formation and lack of snowfall later in the season, which resulted in thicker simulated ice as compared to 2002 (snow depth 0.15±0.03 m). Measured ice thicknesses did not vary significantly at Barrow between years, however (1.64±0.11 m vs. 1.60±0.06 m) which can be explained by a combination of forcing factors not accounted for in our simulations (short- and longwave forcing) or potential differences in ocean heat flux and frazil ice entrainment discussed below.

As indicated by the snow depth PDFs shown in Fig. 9, roughly one fifth of the snow on level ice in 2004 was less than 0.02 m deep, and roughly half less than 0.05 m deep, which explains part of the differences in interannual variations in level ice thickness seen in the ice thickness distributions. Snow depth variations are also likely to

overwhelm differences in ice thicknesses due to variations in other forcing factors. This is evident from Fig. 15(d), which indicates that for snow-free ice, thickness of ice grown for climate normal (1979-2000) conditions is between 0.05 and 0.2 m thicker than that grown for conditions in 2002-2004.

One important factor in determining ice growth rates that is not accounted for in our simple degree-day modeling approach is the retardation of ice growth due to heat transfer from the ocean to the bottom of the ice cover. For the field seasons 2003 and 2004 the ocean heat flux was estimated using measured CTD and current data, in the range of 15 $Wm^{-2}$ in August/September of 2003 in the northern Chukchi Sea, and between 4 and 32 $Wm^{-2}$ in May of 2004 in the southern Chukchi Sea. These values are comparable to estimates from ice-mass balance measurements during the Surface Heat Budget of the Arctic (SHEBA) drift camp in the same area in 1997/98 which indicate that high ocean heat fluxes may have contributed substantially to ice thinning (bottom melt was observed during several episodes throughout winter and spring, McPhee et al, 1998; Perovich et al., 2003). During the SHEBA summer, the ocean heat flux at the bottom of a drifting ice floe was estimated in the range from a few to 40 $Wm^{-2}$ (Perovich et al., 2003). Higher ocean heat fluxes as large as 40 $Wm^{-2}$ were caused by the entrainment of warmer, deeper water as a storm rapidly moved the ice station into

shallower water over the Chukchi Cap (Perovich et al., 2003). At the beginning of bottom melt in late spring, the ocean heat flux amounted to between a few and 10 $Wm^{-2}$ and was approximately 6-7 $Wm^{-2}$ just prior to fall freeze-up (Perovich et al., 2003).

According to a sensitivity study of ice thickness evolution based on field data and thermodynamic modeling, an ocean heat flux of 10 $Wm^{-2}$ would reduce the annual maximum ice thickness down by approximately 0.1 m for first-year landfast ice (Shirasawa et al., 2005). Heat fluxes of between 20 to 30 $Wm^{-2}$ are capable of reducing maximum thickness of undeformed ice by up to 0.4 m. The impact of heat transferred to the ice bottom is also strongly dependent on snow depth, since deep snow cover can push the energy balance at the ice bottom into the melt regime even early in spring. With snow depths below average during the study years 2002-2004, this tends to reduce the sensitivity to ocean heat flux increases. Nevertheless, hydrographic measurements during the SBI cruises indicate a significant reservoir of ocean heat at the top of the halocline (30-50 m) along several sections in the Chukchi and western Beaufort Seas (Codispoti et al., 2005 and submitted). At the end of the ice growth season in 2002, the heat content represented by this water at the top of the halocline was sufficient to melt $0.24 \pm 0.15$ m of ice (14 stations out of a total of 34 along the four major transects in the Chukchi/Beaufort Sea). This is commensurate with observations at the SHEBA ice

camp, where high ocean heat fluxes were thought to be responsible for a net loss of mass over second-year ice during the SHEBA year (Perovich et al., 2003). The thin ice found in the southern Chukchi Sea with modal thicknesses of well below 1 m (Fig. 7) may have been impacted by these high ocean heat fluxes due to effective mixing and transfer of summer water to the base of the ice over the shallow inner shelf. Similarly, multi-year ice modal thicknesses of 2 m or less in the data shown here are small and indicate a significant role for bottom melt, in particular in the absence of thick (>0.3 m) snow cover that could contribute to retardation of ice growth.

The origins of the warm-water layer above the halocline (and potential other heat sources contributing to high winter and ocean spring heat fluxes) are not fully resolved at this point. Based on studies of Chukchi Shelf circulation and mooring data, Shimada et al. (2006) and Woodgate et al. (2006) have argued that increased heat flux through Bering Strait and warmer Chukchi surface waters have significantly contributed to the trend of ice retreat observed in recent years. However, coupled ice-ocean model simulations indicate significant interannual variability in the spreading of Pacific inflow (Maslowski et al., 2000) and suggest that local heating as a result of ice-albedo feedback and interaction between different regional circulation features in the Chukchi Sea contribute significantly to observed ice anomalies as well (Maslowski, pers. comm.

2007). The importance of solar heating and potential trapping of remnant summer water under ice formed in fall is reinforced by a recent study (Perovich et al., 2007), which indicates that the input of solar heat through open water within and outside of the ice pack has approximately doubled in the Chukchi Sea between 1979 and 2005, likely overwhelming any potential signals of increased heat flux through Bering Strait discussed by Woodgate et al. (2006).

### 4.4. Deformation History of the Ice Cover and Contribution of Ice Rafting to Thickening of Level Ice

Origin and circulation of the ice sampled in the SBI study region have been discussed in Section 4.2, with Fig. 12 indicating the broadly shoreparallel motion of the ice pack in 2001/02 and 2003/04 on time scales of several months to a year. However, on shorter timescales, there is a significant shoreward component of ice motion, mostly driven by the surface wind field (Rigor et al., 2002; Rigor and Wallace, 2004) with potential contributions by stresses transmitted through the ice cover as ice concentration increases. In 2003/04 ice advected into the eastern Chukchi from the Beaufort Sea has experienced significant convergence over the course of its drift, even at monthly time

scales (Fig. 12(c)). On shorter time scales, tidal and inertial forcing may result in periodic opening and closing of the pack against the coast, generating new ice under divergent conditions and rafting and ridging this ice under convergent conditions (Kwok et al., 2003; Martin et al., 2004).

The frequent occurrence of rafted ice in level ice sections (Table 2, Fig. 5) suggests that convergent ice deformation episodes may represent an important ice thickening mechanism, at least in the broad (tens to hundreds of kilometers) swath of the Chukchi and Beaufort Seas where the ice cover is directly or indirectly impacted by the presence of a coastline. In contrast with ridging, where fragmentation of ice leads to piling up of blocks, the process of ice rafting can result in significant thickening of ice over large areas without substantial increases in top or bottom roughness as observed here and shown in simulations and laboratory experiments (Hopkins et al., 1999). What is remarkable and in contrast with previous assessments such as that of Babko et al. (2002), is the degree of thickening achieved through this process. In many cases, rafted ice sheet thicknesses exceeded that of the parent ice sheets by factor of 4 or more (as in the example shown in Fig. 5). While rafting has been observed in ice of up to 1 m thickness or more (e.g., Mahoney et al., 2004), it occurs most readily in thin, ductile ice such as nilas.

The geographic distribution of sampling sites during the SBI cruises does not allow for a thorough assessment of the importance of these thickening processes on a regional scale. However, basin-wide analysis of the winter/spring ice deformation field obtained from remote sensing data at high spatial and temporal resolution, indicates that the northern Chukchi and Beaufort Seas do exhibit above-average rates and magnitudes of convergence in the Arctic (Kwok, 2006). While convergence estimates from remote-sensing data are difficult to obtain over the shelf due to the complex circulation patterns, Kwok's analysis shows total net convergences of between 0.1 and 0.5 along the edge of his study area over the outer shelf and adjacent sector of the Canada Basin for the time period November through April. The rafted ice found along the cruise tracks was most likely produced in the environment of the inner shelf, where interaction with the coastline (Mahoney et al., 2004) as well as wind and tidal forcing in a flaw lead or polynya environment favor the production and deformation of thin ice (Martin et al., 2004). This is corroborated by the presence of entrained seafloor sediments in a significant fraction of the rafted ice (Eicken et al., 2005), which indicates formation in waters shallower than about 30 m. Such an interpretation is commensurate with the lack of any significant trend in ice thickness as a function of latitude to the North of the Chukchi and western Beaufort coasts found in this study (Fig. 16).

## 5. Conclusions

(1) In the context of large-scale sea ice change observed in the study region and the sectors of the Arctic Ocean to the North, the measurements of ice thickness reported here are somewhat limited and confined to a region that mostly covers the shelf and does not extent far into the basin. Nevertheless, it is clear that the most prominent signal of large-scale change is expressed in a reduction of overall mean thickness of level ice due to the replacement of multi-year by first-year ice over large areas of the Chukchi and Beaufort Seas (Fig. 1), as discussed previously by, e.g., Tucker et al. (2001) and others. The magnitude of this reduction in level ice thickness is estimated at 0.5 to 1 m over the past two decades, bearing in mind the lack of significant overlap between earlier submarine data and this study (Fig. 13).

(2) The ice-thickness data do not allow any conclusions on the impact of atmospheric warming reported for the study region (Mahoney et al., 2007) over the past several decades, since the magnitude of this signal is masked by variations in snow depth and onset of ice growth (the latter controlled by ocean heat content). However, based on

measured interannual and regional variations in snow depth, it is clear that the snow cover exerts a key influence on the thickness of level ice that can be grown within an ice season and likely dominates the large-scale thermal response of the ice cover to climate variability and change. For the two SBI study years 2002 and 2004, the presence of only a thin snow cover over large areas of the region may in part be responsible for comparatively thick first-year ice observed during the 2004 cruise and in landfast ice at Barrow.

(3) The impact of high ocean heat fluxes on the ice-thickness distribution is difficult to assess based on the ice thickness measurements alone. Ice-growth modeling indicates a significant impact for heat fluxes larger than about 20 $Wm^{-2}$ (Shirasawa et al., 2005), which had been observed during the late-spring cruises as well as at the year-round SHEBA ice camp. In conjunction with recent results from hydrographic surveys during SBI and other studies (Shimada et al., 2006) it appears that relative to conditions of the 1970s and 1980s maximum thicknesses of first-year ice may have been reduced by as much as several decimeters. Given the competing roles of different forcing parameters, a full assessment of the impact of ocean warming on the ice cover requires a process-oriented field or modeling study.

(4) The observed thickness distributions of level ice reflect a significant fraction of rafted ice that was not expressed in a readily detectable fashion in the surface ice morphology (Section 3.2, Table 2). Accounting for the large-scale drift patterns that result in entrainment of this ice in the main pack and considering the large-scale convergence evident from buoy drift and satellite data, it is reasonable to conclude that at least over the shelf rafting can contribute significantly to ice thickening. While existing estimates of large-scale convergence from satellite data support this conclusion (Kwok, 2006), this process needs to be examined in more detail. Rafting can buffer the response of an overall thinner parent ice cover to atmospheric and oceanic warming, by deforming more readily than the thick multi-year ice it replaced in the study region (see also Hibler, 2004). Thus, rafting can compensate for substantial heat input from ocean and atmosphere, such as in the southern Okhotsk Sea, where thermodynamic ice growth results in ice thicknesses of at most around 0.4 m (including snow-ice contribution, Shirasawa et al., 2005) but deformation leads to typical offshore ice pack thicknesses of well above a meter, with individual level floes as thick as 2 m (Toyota et al., 2004; Fukamachi et al., 2006). While rafting may have masked some of the impacts of a warmer climate in the present study, the question remains to what an extent a different

ice deformation regime can help reduce the impacts of warming over larger areas of the shelf. For example, Melling et al. (2005) reached similar conclusions based on their study of a 12-year record of ice draft data obtained at a mooring site on the Mackenzie shelf.

(5) From the perspective of shelf-basin interactions and estimates of biological production in the study region in the context of the SBI project, the results of this study suggest that the light levels controlling growth of ice algae and under-ice phytoplankton may have changed significantly due to the replacement of thick multi-year ice with thinner first-year ice. Furthermore, variations in the onset of fall ice formation and total amount of precipitation can then lead to substantial interannual variations in total snow accumulation on first-year ice, which is also of great importance for under-ice primary production due to its impact on the under-ice light regime (Kirchman et al., this volume; Codispoti et al., this volume). Greater areal fractions of first-year ice are also likely to increase solar heating of the mixed layer under the ice during spring melt (Eicken et al., 2004) and increase the length of the open water season with a reduced ice mass allowing for more rapid spring-time removal of ice, which in turn increases input of solar heat during the open-water phase (Perovich et al., 2007).

**Acknowledgements.**

We thank personnel onboard *USCGC Healy* and *R/V Xuelong* for their professional and friendly support, which enabled us to carry out extensive measurements both on and off the vessels. Rolf Gradinger, Heike Merkel and Michael Tapp helped with field work on the *Healy*. Zhanhai Zhang, Zhijun Li, Chen Bo, Cheng Bin and Pekka Koslof provided helpful support during the CHINARE-2003. Thanks go to Shotaro Uto for his useful comments on EM data analysis and also to anonymous reviewers for their constructive comments to improve the manuscript. This work was supported by the National Science Foundation Grant OPP-0125464 as part of the Shelf-Basin Interactions Program with additional support from the Synthesis of the Arctic System program grant OPP-0531173, by the Ministry of Finance of China as part of the Second Chinese National Arctic Research Expedition (CHINARE−2003), organized by the Chinese Arctic and Antarctic Administration (CAA), by the National Institute of Polar Research in Japan, by the Japan Society for the Promotion of Science and by the Japanese Ministry of Education, Culture, Sports, Science and Technology.

**References**

Babko, O., Rothrock, D.A., Maykut, G.A., 2002. Role of rafting in the mechanical redistribution of sea ice thickness. Journal of Geophysical Research 107(C10), 1029/JC000190.

Codispoti, L.A., Flagg, C., Kelly, V., Swift, J.H., 2005. Hydrographic conditions during the 2002 SBI process experiments. Deep-Sea Research Part II 52, 3199-3226.

Codispoti, L.A., Flagg, C.N., Swift, J.H., this volume. Hydrographic conditions during the 2004 SBI process experiments. Submitted to Deep-Sea Research.

Comiso, J.C., 2002. A rapidly declining perennial sea ice cover in the Arctic. Geophysical Research Letters 29(20), 1956, doi:10.1029/2002GL015650.

Eicken, H., 2003. From the microscopic to the macroscopic to the regional scale: Growth, microstructure and properties of sea ice. In: Thomas, D.N., Dieckmann, G..S. (Eds.), Sea ice - An introduction to its physics, biology, chemistry and geology. Blackwells Scientific Ltd., London, pp. 22-81.

Eicken, H., Tucker III, W.B., Perovich, D.K., 2001. Indirect measurements of the mass balance of summer Arctic sea ice with an electromagnetic induction technique. Annals of Glaciology 33, 194-200.

Eicken, H., Krouse, H.R., Kadko, D., Perovich, D.K., 2002. Tracer studies of pathways and rates of meltwater transport through Arctic summer sea ice. Journal of Geophysical Research 107(C10), doi:10.1029/2000JC000583.

Eicken, H., Grenfell, T.C., Perovich, D.K., Richter-Menge, J.A., Frey, K., 2004. Hydraulic controls of summer Arctic pack ice albedo. Journal of Geophysical Research 109(C08007), doi:10.1029/2003JC001989.

Eicken, H., Gradinger, R., Gaylord, A., Mahoney, A., Rigor, I., Melling, H., 2005. Sediment transport by sea ice in the Chukchi and Beaufort Seas: Increasing importance due to changing ice conditions ? Deep-Sea Research Part II 52, 3281-3302.

Ezraty, R., Cavanie, A., 1999a. Construction and evaluation of 12.5 km grid NSCAT

backscatter maps over Arctic sea ice. IEEE Transactions on Geoscience and Remote Sensing 37, 1685-1697.

Ezraty, R., Cavanie, A., 1999b. Intercomparison of backscatter maps over Arctic sea ice from NSCAT and the ERS scatterometer. Journal of Geophysical Research 104(C5), 11471-11483.

Fukamachi, Y., Mizuta, G., Ohshima, K.I., Toyota, T., Kimura, N., Wakatsuchi, M., 2006. Sea ice thickness in the southwestern Sea of Okhotsk revealed by a moored ice-profiling sonar. Journal of Geophysical Research 111(C09018), doi:10.1029/2005JC003327.

Gloersen, P., Campbell, W.J., Cavalieri, D.J., Comiso, J.C., Parkinson, C.L., Zwally, H.J., 1992. Arctic and Antarctic sea ice, 1978-1987: Satellite passive-microwave observations and analysis. NASA Special Publication SP-511, 290pp.

Gradinger, R., this volume. Sea ice algae: major contributors to primary production and algal biomass in the Chukchi and Beaufort Sea during May/June 2002. Deep Sea Research II.

Grebmeier, J.M., Harvey, H.R., 2005. The Western Arctic Shelf-Basin Interactions (SBI) project: An overview. Deep-Sea Research Part II 52, 3109-3115.

Haas, C., 1998. Evaluation of ship–based electromagnetic–inductive thickness measurements of summer sea–ice in the Bellingshausen and Amundsen Seas, Antarctica. Cold Regions Science and Technology 27, 1−16.

Haas, C., Gerland, S., Eicken, H., Miller, H., 1997. Comparison of sea–ice thickness measurements under summer and winter conditions in the Arctic using a small electromagnetic induction device. Geophysics 62, 749−757.

Haas, C., Eicken, H., 2001. Interannual variability of summer sea ice thickness in the Siberian and central Arctic under different atmospheric circulation regimes. Journal of Geophysical Research 106(C3), 4449-4462.

Hibler III, W.D., 2004. Modelling the dynamic response of sea ice. In Bamber, J.L., Payne, A.J. (Eds.), Mass balance of the cryosphere: Observations and modelling of

contemporary and future changes. Cambridge University Press, Cambridge, pp. 227-334.

Hopkins, M.A., Tuhkuri, J., Lensu, M., 1999. Rafting and ridging of thin ice sheets. Journal of Geophysical Research 104(C6), 13605-13613.

Kirchman, D.L., Hill, V., Cottrell, M.T., Gradinger, R., Malmstrom, R.R., Parker, A., this volume. Standing stocks, production, and respiration of phytoplankton and heterotrophic bacteria in the western Arctic Ocean. Submitted to Deep-Sea Research.

Kovacs, A., Valleau, N.C., Holladay, J.C., 1987. Airborne electromagnetic sounding sea-ice thickness and subice bathymetry. Cold Regions Science and Technology 14, 289-311.

Kovacs, A., Holladay, J.S., Bergerson, Jr., C.J., 1995. The footprint/altitude ratio for helicopter electromagnetic sounding of sea-ice thickness: comparison of theoretical and field estimates. Geophysics 60(2), 374-380.

Kwok, R., 2006. Contrasts in sea ice deformation and production in the Arctic seasonal and perennial ice zones. Journal of Geophysical Research 111(C11S22),doi:10.1029/2005JC003246.

Kwok, R., Cunningham, G.F., Hibler III, W.D., 2003. Sub-daily sea ice motion and deformation from RADARSAT observations. Geophysical Research Letters 30(23), 2218, doi:10.1029/2003GL018723.

Lange, M.A., Eicken, H., 1991. The sea ice thickness distribution in the northwestern Weddell Sea. Journal of Geophysical Research 96(C3), 4821-4837.

Mahoney, A., Eicken, H., Shapiro, L.H., Grenfell T.C., 2004. Ice motion and driving forces during a spring ice shove on the Alaskan Chukchi coast. Journal of Glaciology 50, 195-207.

Mahoney, A., Eicken, H., Graves, A., Shapiro, L., 2007. Alaska landfast sea ice: Links with bathymetry and atmospheric circulation. Journal of Geophysical Research 112(C02001), doi:10.1029/2006JC003559.

Martin, S., Drucker, R., Kwok, R., Holt, B., 2004. Estimation of the thin ice thickness and heat flux for the Chukchi Sea Alaskan coast polynya from Special Sensor Microwave/Image data, 1990-2001. Journal of Geophysical Research 109(C10012), doi:10.1029/2004JC002428.

Maslowski, W., Newton, B., Schlosser, P., Semtner, A., Martinson, D., 2000. Modeling recent climate variability in the Arctic Ocean. Geophysical Research Letters 27(22), 3743-3746.

Maykut, G.A., 1986. The surface heat and mass balance. In: Untersteiner, N. (Ed.), The Geophysics of Sea Ice. Martinus Nijhoff Publ., Dordrecht (NATO ASI B146), pp. 395-463.

McNeill, J.D., 1980. Electromagnetic terrain conductivity measurements at low induction numbers. Geonics Limited Technical Note, TN–6, 15 pp.

McPhee, M.G., Stanton, T.P., Morison, J.H., Martinson, D.G., 1998. Freshening of the

upper ocean in the Arctic: Is perennial sea ice disappearing? Geophysical Research Letters 25(10), 1729-1732.

Melling, H., Riedel, D.A., Gedalof, Z., 2005. Trends in the draft and extent of seasonal pack ice, Canadian Beaufort Sea. Geophysical Research Letters 32(L24501), doi:10.1029/2005GL024483.

National Snow and Ice Data Center. 1998, updated 2006. Submarine upward looking sonar ice draft profile data and statistics. Boulder, CO: National Snow and Ice Data Center/World Data Center for Glaciology. Digital media.

Perovich, D.K., Grenfell, T.C., Richter-Menge, J.A., Light, B., Tucker III, W.B., Eicken, H., 2003. Thin and thinner: Sea ice mass balance measurements during SHEBA. Journal of Geophysical Research 108(C3), 8050, doi:10.1029/2001JC001079.

Perovich, D.K., Light, B., Eicken, H., Jones, K.F., Runciman, K., Nghiem, S.V., 2007. Increasing solar heating of the Arctic Ocean and adjacent seas, 1979-2005: Attribution and role in the ice-albedo feedback. Geophysical Research Letters 34(L19505),

doi:10.1029/2007GL031480.

Pfirman, S., Haxby, W., Eicken, H., Jeffries, M., Bauch, D., 2004. Drifting Arctic sea ice archives changes in ocean surface conditions. Geophysical Research Letters 31(L19401), doi:10.1029/2004GL020666.

Reid, J.E., Worby, A.P., Vrbancich, J., Munro, A.I.S., 2003. Ship–borne electromagnetic measurement of Antarctic sea–ice thickness. Geophysics 68, 1537−1546.

Reid, J.E., Vrbancich, J., 2004. A comparison of the inductive–limit footprints of airborne electromagnetic systems. Geophysics 69, 1229–1239.

Reid, J.E., Pfaffling, A., Vrbancich, J., 2006, Airborne electromagnetic footprints in 1D earths. Geophysics 71, G63-G72.

Rigor, I.G., Wallace, J.M., Colony, R.L., 2002. Response of sea ice to the Arctic Oscillation, Journal of Climate 15, 2648-2663.

Rigor, I.G., Wallace, J.M., 2004. Variations in the age of Arctic sea-ice and summer sea-ice extent. Geophysical Research Letters 31(L09401),doi:10.1029/2004GL019492.

Rothrock, D.A., Thorndike, A.S., 1980. Geometric properties of the underside of sea ice. Journal of Geophysical Research 85(C7), 3955-3963.

Rothrock, D.A., Yu, Y., Maykut, G.A., 1999. Thinning of the Arctic Sea-ice cover. Geophysical Research Letters 26(23), 3469-3472.

Serreze, M.C., Holland, M.M., Stroeve, J., 2007. Perspectives on the Arctic's shrinking sea-ice cover. Science 315, 1533-1536.

Shimada, K., Kamoshida, T., Itoh, M., Nishino, S., Carmack, E., McLaughlin, F.A., Zimmermann, S., Proshutinsky, A., 2006. Pacific Ocean inflow: Influence on catastrophic reduction of sea ice cover in the Arctic Ocean. Geophysical Research Letters 33(L08605), doi:10.1029/2005GL025624.

Shirasawa, K., Leppäranta, M., Saloranta, T., Kawamura, T., Polomoshnov, A., Surkov, G., 2005. The thickness of coastal fast ice in the Sea of Okhotsk. Cold Regions Science

and Technology 42, 25-40.

Shirasawa, K., Tateyama, K., Takatsuka, T., Kawamura, T., Uto, S., 2006. Ship-borne electromagnetic induction sounding of sea ice thickness in the Arctic during the summer 2003. Polar Meteorology and Glaciology 20, 53-62.

Tateyama, K., Uto, S., Shirasawa, K., Enomoto, H., 2004. Electromagnetic-inductive measurements for the undeformed and deformed sea-ice and snow in the East Antarctic. The Proceedings of the 14th ISOPE Conference, Toulon, France, 806-812.

Tateyama, K., Shirasawa, K., Uto, S., Kawamura, T., Toyota T., Enomoto, H., 2006. Standardization of electromagnetic–induction measurements of sea–ice thickness in polar and subpolar seas. Annals of Glaciology 44, 240-246.

Tin, T., Jeffries, M.O., 2003. Morphology of deformed first-year sea ice features in the Southern Ocean. Cold Regions Science and Technology 36, 141-163.

Toyota, T., Kawamura, T., Ohshima, K.I., Shimoda, H., Wakatsuchi, M., 2004.

Thickness distribution, texture and stratigraphy, and a simple probabilistic model for dynamical thickening of sea ice in the southern Sea of Okhotsk. Journal of Geophysical Research 109(C06001), doi:10.1029/2003JC002090.

Tucker, W.B.I., Weatherly, J.W., Eppler, D.T., Farmer, D., Bentley, D.L., 2001. Evidence for the rapid thinning of sea ice in the western Arctic Ocean at the end of the 1980s. Geophysical Research Letters 28(14), 2851-2854.

Uto, S., Shimoda, H., Tamura, K., 1999. Ship-based sea ice observations in the southernmost part of the Sea of Okhotsk. Proceedings of the 15th POAC, 1, 380-388.

Uto, S., Shimoda, H., Izumiyama, K., 2002. Ship–based sea ice observations in Lützow–Holm Bay, east Antarctica. Proceedings of the 16th IAHR Symposium, Dunedin, New Zealand, 218−224.

Uto, S., Toyota, T., Shimoda, H., Tateyama, K., Shirasawa, K., 2006. Ship-borne electromagnetic induction sounding of sea-ice thickness in the southern Sea of Okhotsk. Annals of Glaciology 44, 253-260.

Wadhams, P., 1998. Sea ice morphology. In: Leppäranta, M. (Ed.), Physics of Ice-Covered Waters, Vol. 1, Helsinki University Press, Helsinki, pp. 231-288.

Woodgate, R.A., Aagaard, K., Weingartner, T.J., 2006. Interannual changes in the Bering Strait fluxes of volume, heat and freshwater between 1991 and 2004. Geophysical Research Letters 33(L15609), doi:10.1029/2006GL026931.

Worby, A.P., Lytle, V.I., Massom, R.A., 1999. On the use of electromagnetic induction sounding to determine winter and spring sea ice thickness in the Antarctic. Cold Regions Science and Technology 29, 49−58.

**Figure Captions:**

Figure 1. Maps of the study region showing the measurements locations in (a) May/June 2002, (b) August/September 2003 and (c) May/June 2004 with the National Snow and Ice Data Center's mean ice concentrations (in 0 to 1, see color scale) during the periods from 10 May to 9 June 2002, from 24 August to 7 September 2003 and from 20 May to

20 June 2004,; ice concentrations (in %, see color scale) from AMSR-E images on (d) 1 June 2002, (e) 1 September 2003 and (f) 1 June 2004; and (g), (h) and (i) QuikSCAT radar backscatter maps, indicating the distribution of multiyear ice in the study region immediately prior to the onset of surface melt.

Figure 2. A schematic of SEM ice thickness measurements.

Figure 3. (a) Observed apparent conductivity versus drill-hole total thickness (from direct thickness measurements) in 2002, 2003 and 2004, and (b) IEM total thickness versus drill-hole total thickness for level and deformed ice in 2002, 2003 and 2004. Black and grey solid lines in (b) show regression lines of level ice (y=0.77x+0.47, with the correlation coefficient of 0.74) and deformed ice (y=0.70x+0.59, with the correlation coefficient of 0.82), respectively.

Figure 4. Salinity and $\delta^{18}$O profile in the ice core, measured (a) at the ice floe (70.67$^{o}$N, 167.31$^{o}$W) on 12 May 2002, (b) at the ice floe (78$^{o}$19'N, 148$^{o}$2'W) on 22 August 2003, and (c) salinity profile at the ice floe (71$^{o}$55'N, 154$^{o}$51'W) on 16 June 2004; and Salinity and temperature profile below the ice, measured (d), (e) and (f) at the

corresponding ice floes to (a), (b) and (c), respectively. In (b), ●, +, ⊕, ⊗, ✧ and ★ show values for ice salinity, ice $\delta^{18}O$, water salinity, water $\delta^{18}O$, snow salinity and snow $\delta^{18}O$, respectively.

Figure 5. Stratigraphic cross-section of a level ice floe turned on its side along icebreaker hull (top is up, scale bar is 0.5 m). Note the multiple rafts stacked on top one another, with the lower rafts associated with sediment particles entrained into the ice cover during growth.

Figure 6: Typical profiles of total thickness (snow + ice), measured in (a) 2002, (b) 2003 and (c) 2004 by means of drilling and IEM measurements.

Figure 7. Comparison of ice thickness probability density functions (PDFs) derived for level and deformed ice from IEM measurements in 2002, 2003 and 2004. The bin size is 0.1 m.

Figure 8. Comparison of ice thickness probability density functions (PDFs) derived from IEM measurements in 2002, 2003 and 2004 for level ice. The bin size is 0.1 m.

Figure 9. Probability density functions (PDFs) for snow depth on level ice in 2002 and 2004. The bin size is 0.02 m.

Figure 10. SEM total thickness and ice concentration with time in day (a) starting from 24 August 2003 along the *R/V Xuelong* cruise track, and (b) starting from 20 May 2004 along the *USCGC Healy* cruise track. Ice concentration (in %) was estimated from the open water area detected by the laser distance meter at the 1-sec interval over the 1-min measurement period.

Figure 11. Comparison of total thickness probability density functions (PDFs) derived from SEM measurements in 2003 and 2004. The bin size is 0.1 m.

Figure 12. Trajectories of ice drift buoys covering the study area during the period (a) from October 2001 to August 2002, (b) from January 2003 to September 2003, and (c) from January 2003 to July 2004. Data have been obtained from the International Arctic Buoy Program (http://iabp.apl.washington.edu/).

Figure 13. Cruise tracks of submarine sonar measurements of ice draft and SEM total

thickness measurements. Shown are tracks by 1986, 1987, 1988, 1989, 1990, 1991, 1992, 1993 and 1994 submarine and by 2003 and 2004 SEM measurements. The colors for each line correspond to those in Fig. 14.

Figure 14. Comparison of total thickness probability density functions (PDFs) derived from submarine sonar measurements of ice draft (converted to ice thickness by multiplying by 1.08 following Wadhams (1998), for spring sea ice of 910 kg $m^{-3}$ density) for (a) 1986, 1987, 1988 and 1989; (b) 1990, 1991, 1992, 1993 and 1994; and (c) SEM measurements in 2003 and 2004; and (d) IEM measurements for level ice in 2002, 2003 and 2004. Submarine sonar data have been obtained from the National Snow and Ice Data Center (2006). The bin size is 0.1 m.

Figure 15. Results of ice-growth simulations with a freezing-degree day model for the ice seasons 2001/02 (A), 2002/03 (B), 2003/04 (C) and climate normals (1979-2000, D). Different curves represent different days of onset of ice formation and different snow depths. Thick, dashed lines indicate conditions as found for Barrow landfast ice in 2001/02 and 2003/04.

Figure 16. EM-derived total thickness (mean for individual stations or track segments) plotted as a function of latitude.

**Tables**

Table 1. Mean and modal ice and snow thickness by drill hole profiling and IEM/SEM measurements in the Chukchi Sea in 2002, 2003 and 2004.

Table 2. Fraction of deformed ice from ship-based observations of ice stratigraphy.

Table 1. Mean and Modal Ice and Snow Thickness by Drill Hole Profiling and IEM/SEM Measurements in the Chukchi Sea in 2002, 2003 and 2004

| | | | Drill Hole Measurements | | | | | IEM Measurements | | | Level ice | | Deformed ice | | SEM Measurements | | |
|---|---|---|---|---|---|---|---|---|---|---|---|---|---|---|---|---|---|
| Project, Date, ddmmyy | Approximate Location | Ice St. No. | No. of Hole | Distance, m | Ice Thickness*, m | Freeboard*, m | Draft*, m | Snow Depth*, m | Profile Length, m | Meas. Spacing, m | Ice Thickness*, m | Snow Depth*, m | Ice Thickness*, m | Snow Depth*, m | Area, Latitude, Longitude | Total Length, hour | Primary Mode, (Sec. Mode), m |
| SBI-02 | | | | | | | | | | | | | | | | | |
| 100502 | 67°30'N, 168°52'W | 020510 | 8 | 510 | 1.32±1.11 | 0.06±0.07 | 1.11±1.05 | 0.24±0.16 | 510 | 5 | 1.41±0.87 | 0.20±0.13 | 1.71±0.68 | 0.32±0.19 | | | |
| 120502 | 70°40'N, 167°18'W | 020512 | 6 | 530 | 1.54±1.47 | 0.05±0.03 | 1.50±1.48 | 0.23±0.15 | 530 | 5 | 1.10±0.55 | 0.19±0.09 | 2.15±0.76 | 0.35±0.21 | | | |
| 140502 | 71°51'N, 166°01'W | 020514 | 0 | 360 | - | - | - | 0.33±0.23 | 360 | 5 | 2.07±1.02 | 0.22±0.19 | 3.22±1.55 | 0.35±0.22 | | | |
| 160502 | 72°42'N, 161°14'W | 020516 | 0 | 500 | - | - | - | 0.16±0.10 | 500 | 5 | 0.82±0.34 | 0.14±0.06 | 1.49±0.49 | 0.25±0.17 | | | |
| 170502 | 72°54'N, 160°30'W | 020517 | 0 | 100 | 1.24±0.63 | 0.08±0.02 | 1.16±0.61 | 0.15±0.09 | 100 | 5 | 2.03±0.75 | 0.14±0.07 | 2.98±1.64 | 0.13±0.07 | | | |
| 190502 | 73°20'N, 160°20'W | 020519 | 6 | 300 | 1.67±0.09 | 0.14±0.02 | 1.53±0.08 | 0.20±0.16 | 300 | 5 | 1.79±0.34 | 0.16±0.09 | 1.92±0.95 | 0.26±0.11 | | | |
| 210502 | 73°44'N, 158°56'W | 020521 | 3 | 500 | 2.71±1.56 | 0.23±0.22 | 2.07±1.26 | 0.18±0.12 | 500 | 5 | 2.25±1.01 | 0.17±0.12 | 3.19±1.45 | 0.18±0.13 | | | |
| 230502 | 73°28'N, 157°40'W | 020523 | 7 | 500 | 0.57±0.02 | 0.03±0.01 | 0.54±0.02 | 0.14±0.11 | 500 | 5 | 1.70±0.73 | 0.13±0.10 | 2.74±1.58 | 0.17±0.15 | | | |
| 250502 | 73°05'N, 158°12'W | 020525 | 3 | 790 | 1.71±0.07 | 0.16±0.01 | 1.55±0.06 | 0.06±0.05 | 790 | 5 | 1.73±0.22 | 0.06±0.05 | 2.23±0.61 | 0.10±0.06 | | | |
| 270502 | 72°52'N, 158°03'W | 020527 | 2 | 260 | 1.77±0.09 | 0.16±0.01 | 1.62±0.08 | 0.06±0.06 | 260 | 5 | 1.79±0.23 | 0.06±0.06 | - | - | | | |
| 290502 | 72°36'N, 158°46'W | 020529 | 0 | 175 | - | - | - | 0.09±0.15 | 175 | 5 | 1.76±0.40 | 0.02±0.01 | 2.55±0.82 | 0.19±0.20 | | | |
| 300502 | 72°14'N, 159°50'W | 020530 | 2 | 545 | - | - | - | 0.06±0.06 | 545 | 5 | 1.06±0.42 | 0.05±0.03 | 1.54±1.00 | 0.07±0.08 | | | |
| 030602 | 71°29'N, 153°53'W | 020603 | 3 | 1035 | 1.40±0.06 | 0.16±0.02 | 1.24±0.09 | 0.08±0.06 | 1035 | 5 | 1.63±0.44 | 0.09±0.06 | 2.94±1.11 | 0.07±0.04 | | | |
| 050602 | 72°04'N, 154°27'W | 020605 | 2 | 300 | 1.78±0.53 | 0.18±0.08 | 1.61±0.46 | 0.06±0.04 | 300 | 2.5 | 1.16±0.35 | 0.05±0.04 | 1.48±0.56 | 0.07±0.05 | | | |
| 090602 | 72°33'N, 154°38'W | 020609 | 0 | 530 | - | - | - | 0.07±0.06 | 530 | 5 | 1.76±0.37 | 0.06±0.07 | 2.95±1.10 | 0.08±0.07 | | | |
| CHINARE-2003 | | | | | | | | | | | | | | | 76-81°N | 175 | |
| 110803 | 74°41'N, 164°04'W | | 41 | 121 | 1.91±0.50 | 0.24±0.07 | 1.71±0.54 | | | | | | | | 144-173°W | | |
| 130803 | 75°29'N, 152°51'W | | 21 | 100 | 1.93±0.85 | 0.30±0.12 | 1.63±0.80 | | | | | | | | | | |
| 200803 | 77°31'N, 152°22'W | Ice St. 1 | 21 | 100 | 1.90±0.56 | 0.22±0.05 | 1.46±0.55 | 0.26±0.24 | 100 | 1 | 1.51±0.31 | | - | - | | | |
| 260803 | 78°19'N, 148°06'W | | 21 | 100 | 1.40±0.10 | 0.24±0.05 | 1.16±0.08 | | | | | | | | | | |
| 310803 | 78°42'N, 144°43'W | Ice St. 2 | 107 | 2207 | 1.72±0.51 | 0.30±0.13 | 1.42±0.43 | 0.29±0.12 | 2207 | 2 | 1.70±0.44 | | 2.29±0.77 | | | | |
| 060903 | 77°30'N, 162°29'W | Ice St. 3 | 21 | 200 | 1.37±1.05 | 0.27±0.33 | 1.09±0.77 | 0.08±0.04 | 200 | 2 | 1.58±0.82 | | 2.73±0.80 | | | | 0.1,1.1, (1.4) |
| SBI-04 | | | | | | | | | | | | | | | 68-74°N | 436 | |
| 210504 | 70°40'N, 167°13'W | 040521 | 5 | 505 | 0.99±0.36 | 0.08±0.02 | 0.91±0.35 | 0.05±0.06 | 505 | 5 | 1.18±0.63 | 0.04±0.05 | 1.62±0.69 | 0.06±0.08 | 154-169°W | | |
| 240504 | 72°00'N, 159°46'W | 040524 | 4 | 530 | 2.74±0.81 | 0.28±0.10 | 2.52±0.71 | 0.16±0.16 | 530 | 5 | 2.70±0.52 | 0.16±0.18 | 2.76±0.79 | 0.17±0.14 | | | |
| 260504 | 72°04'N, 159°36'W | 040526 | 4 | 530 | 2.07±0.24 | 0.17±0.04 | 1.90±0.21 | 0.20±0.21 | 530 | 5 | 2.14±0.34 | 0.17±0.19 | 2.76±0.60 | 0.36±0.29 | | | |
| 310504 | 72°43'N, 158°24'W | 040531 | 5 | 625 | 1.89±0.21 | 0.25±0.02 | 1.68±0.20 | 0.21±0.12 | 625 | 5 | 1.95±0.23 | 0.17±0.12 | 2.71±0.72 | 0.33±0.16 | | | |
| 020604 | 72°51'N, 158°12'W | 040602 | 4 | 250 | 1.66±0.80 | 0.12±0.08 | 1.54±0.73 | 0.16±0.07 | 250 | 5 | 2.06±0.14 | 0.16±0.06 | 1.74±0.85 | 0.14±0.15 | | | |
| 040604 | 73°08'N, 157°47'W | 040604 | 4 | 730 | 1.98±0.02 | 0.21±0.07 | 1.77±0.05 | 0.04±0.04 | 730 | 5 | 1.91±0.16 | 0.05±0.06 | 3.29±1.11 | 0.12±0.12 | | | |
| 110604 | 71°41'N, 154°47'W | 040611 | 1 | 200 | 0.95 | 0.11 | 0.84 | 0.05±0.03 | 200 | 5 | 1.22±0.37 | 0.05±0.03 | 1.98±0.56 | 0.04±0.01 | | | |
| 140604 | 72°15'N, 154°29'W | 040614 | 4 | 435 | 1.64±0.47 | 0.08±0.03 | 1.56±0.45 | 0.05±0.06 | 435 | 5 | 1.52±0.56 | 0.04±0.04 | 3.31±1.13 | 0.12±0.12 | | | |
| 160604 | 71°55'N, 154°51'W | 040616 | 4 | 590 | 1.72±0.57 | 0.08±0.12 | 1.66±0.50 | 0.08±0.04 | 590 | 5 | 1.60±0.12 | 0.05±0.05 | 1.48±0.37 | 0.02±0.02 | | | 0.7, (1.4) |

* Mean ± Standard Deviation

Table 2: Fraction of deformed ice from ship-based observations of ice stratigraphy

| Expedition | Total obs. | Locations | Deformed ice obs. | Def. ice locations |
|---|---|---|---|---|
| SBI 2002 | 48 | 28 | 31 (64%) | 16 (57%) |
| SBI 2004 | 64 | 50 | 23 (34%) | 21 (42%) |

Locations refers to all observations made within one 10 min. standard observation period (corresponding to 1-2 km of ship track typically). Fraction of deformed ice observations as part of total given in parentheses.

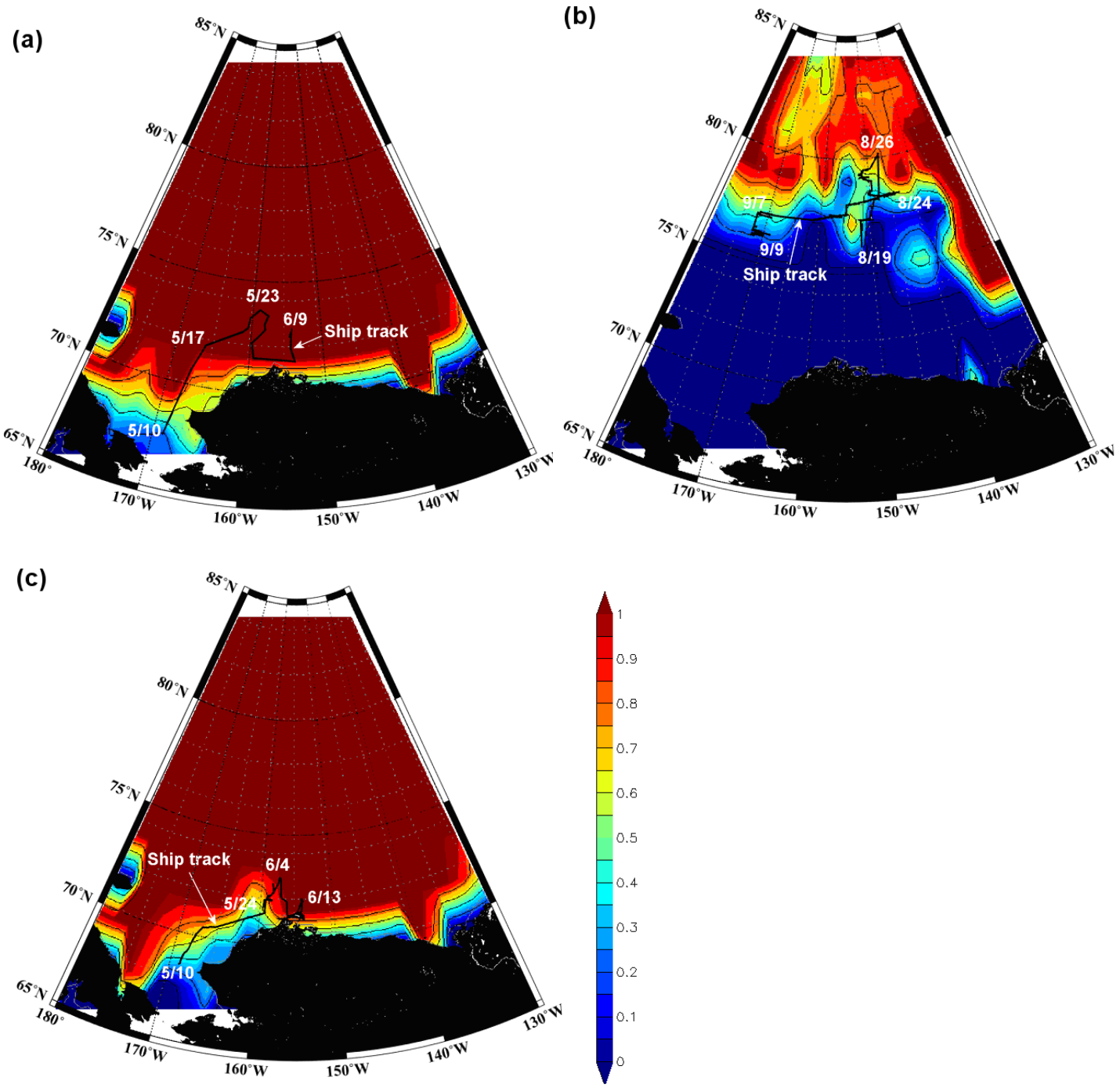
(a)
85°N
80°N
75°N
70°N
65°N
180°
170°W
160°W
150°W
140°W
130°W
5/23
6/9
Ship track
5/17
5/10
(b)
8/26
8/24
8/7
9/9
8/19
Ship track
(c)
Ship track
6/4
5/24
6/13
5/10
1
0.9
0.8
0.7
0.6
0.5
0.4
0.3
0.2
0.1
0

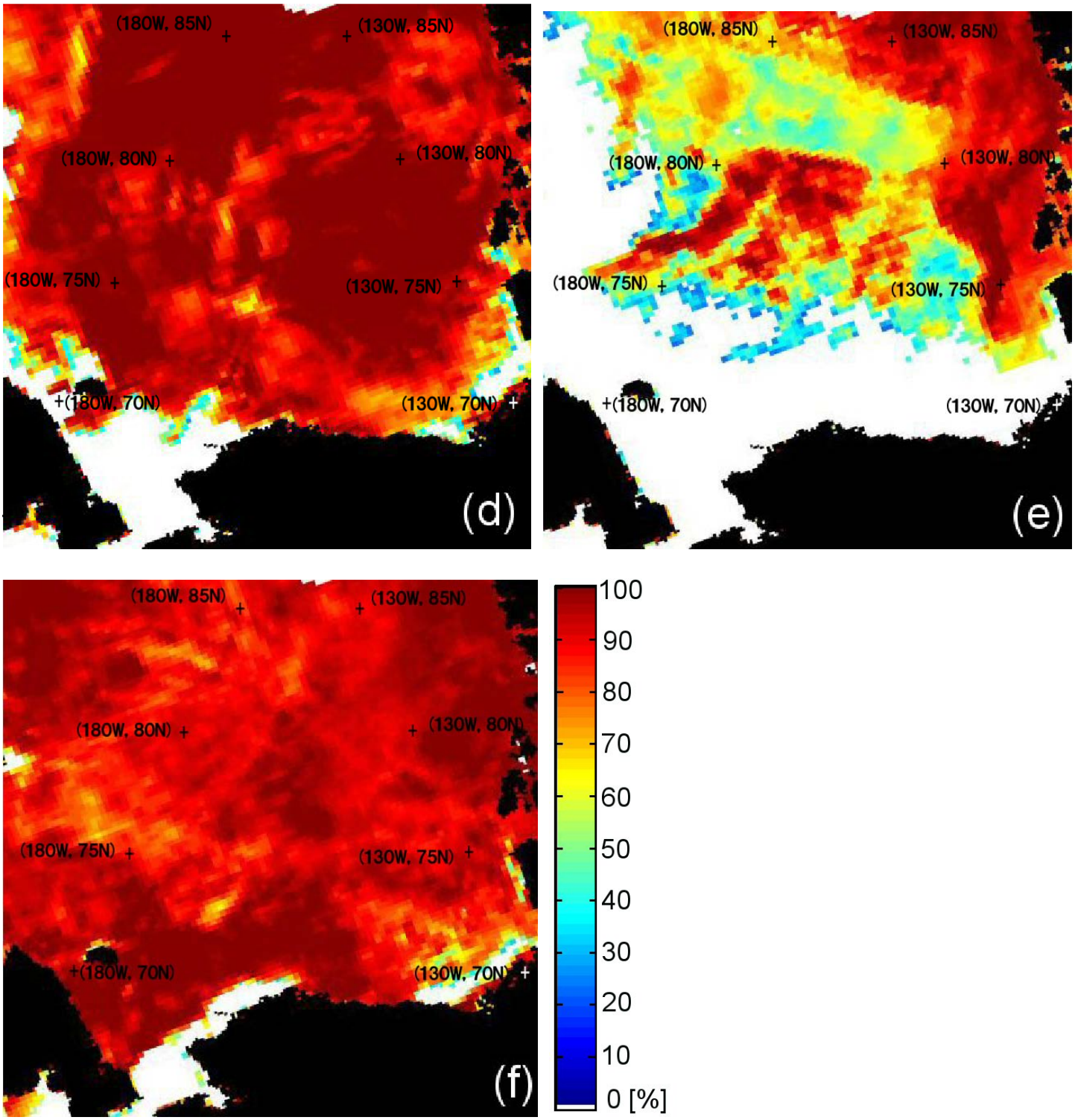


Figure 1. (a), (b), (c), (d), (e) and (f)

Sea-ice thickness variability in the Chukchi Sea, spring and summer 2002-2004
Shirasawa et al.

(g)

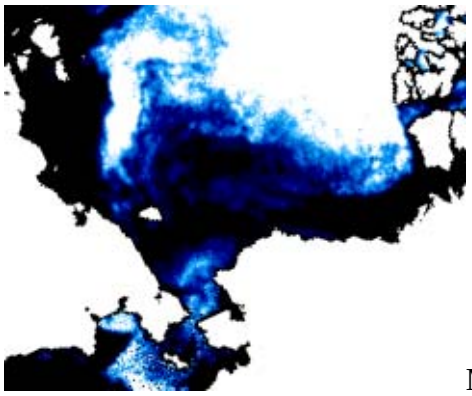

May 1, 2002

(h)

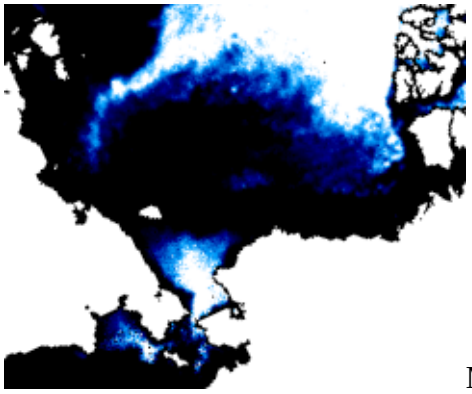

May 1, 2003

(i)

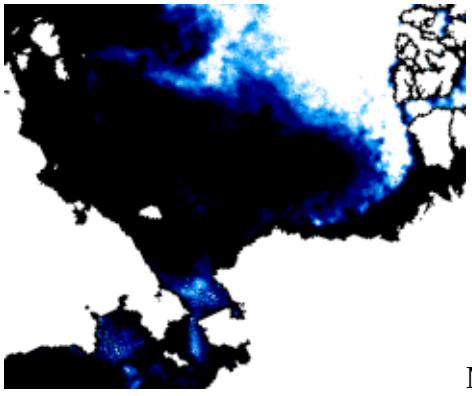

May 1, 2004

Figure 1. (g), (h) and (i).

Sea-ice thickness variability in the Chukchi Sea, spring and summer 2002-2004
Shirasawa et al.

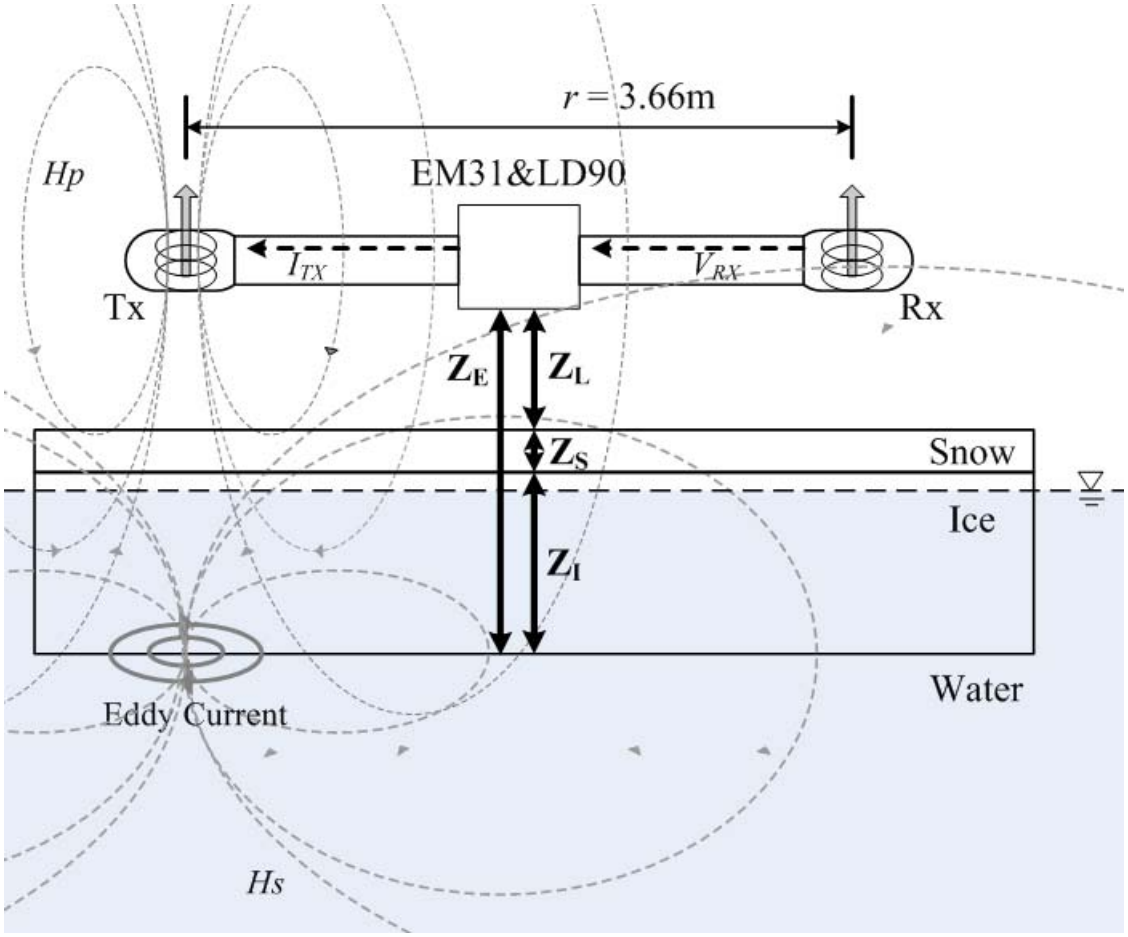


Figure 2. A schematic of SEM ice thickness measurements.

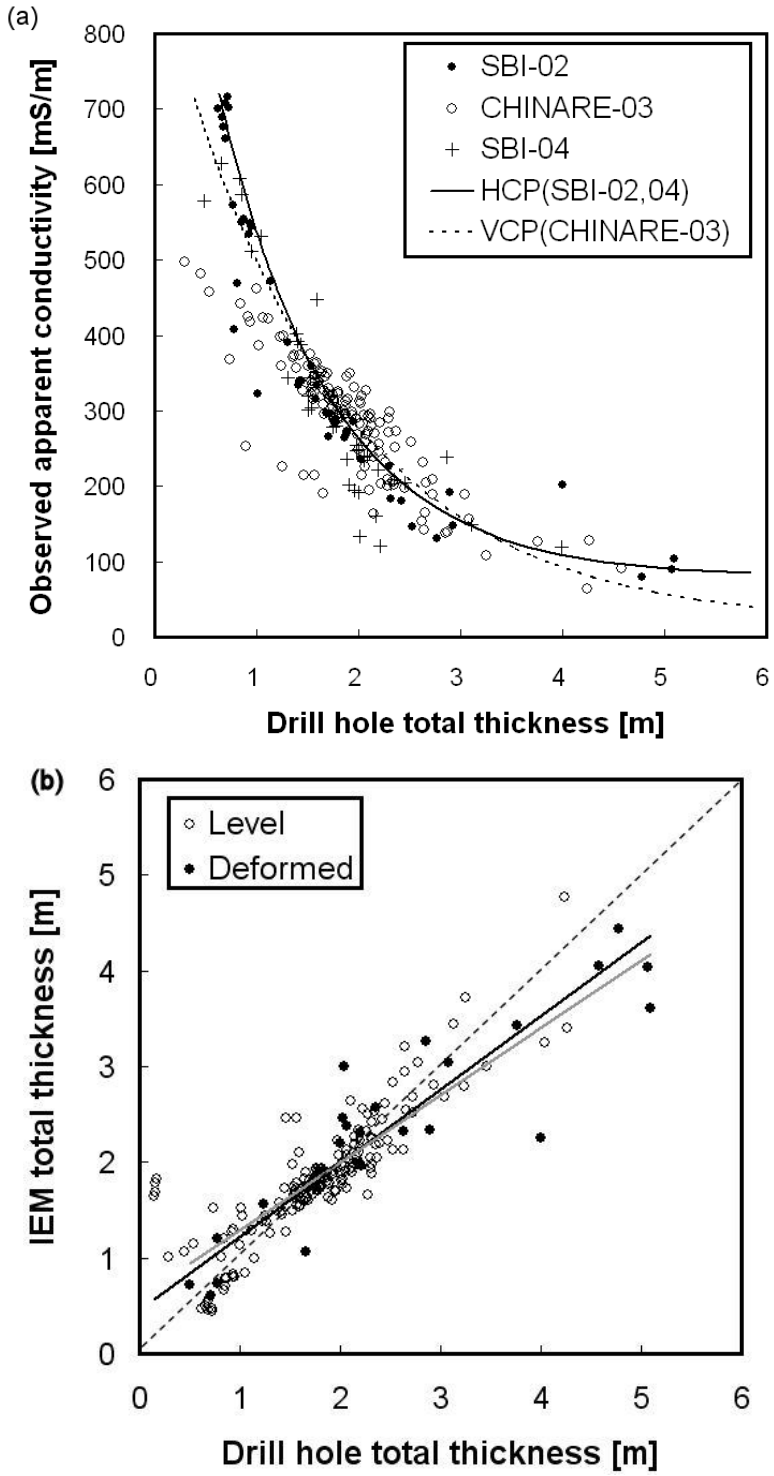


Figure 3. (a) Observed apparent conductivity versus drill-hole total thickness (from direct thickness measurements) in 2002, 2003 and 2004, and (b) IEM total thickness versus drill-hole total thickness for level and deformed ice in 2002, 2003 and 2004. Black and grey solid lines in (b) show regression lines of level ice (y=0.77x+0.47, with the correlation coefficient of 0.74) and deformed ice (y=0.70x+0.59, with the correlation coefficient of 0.82), respectively.

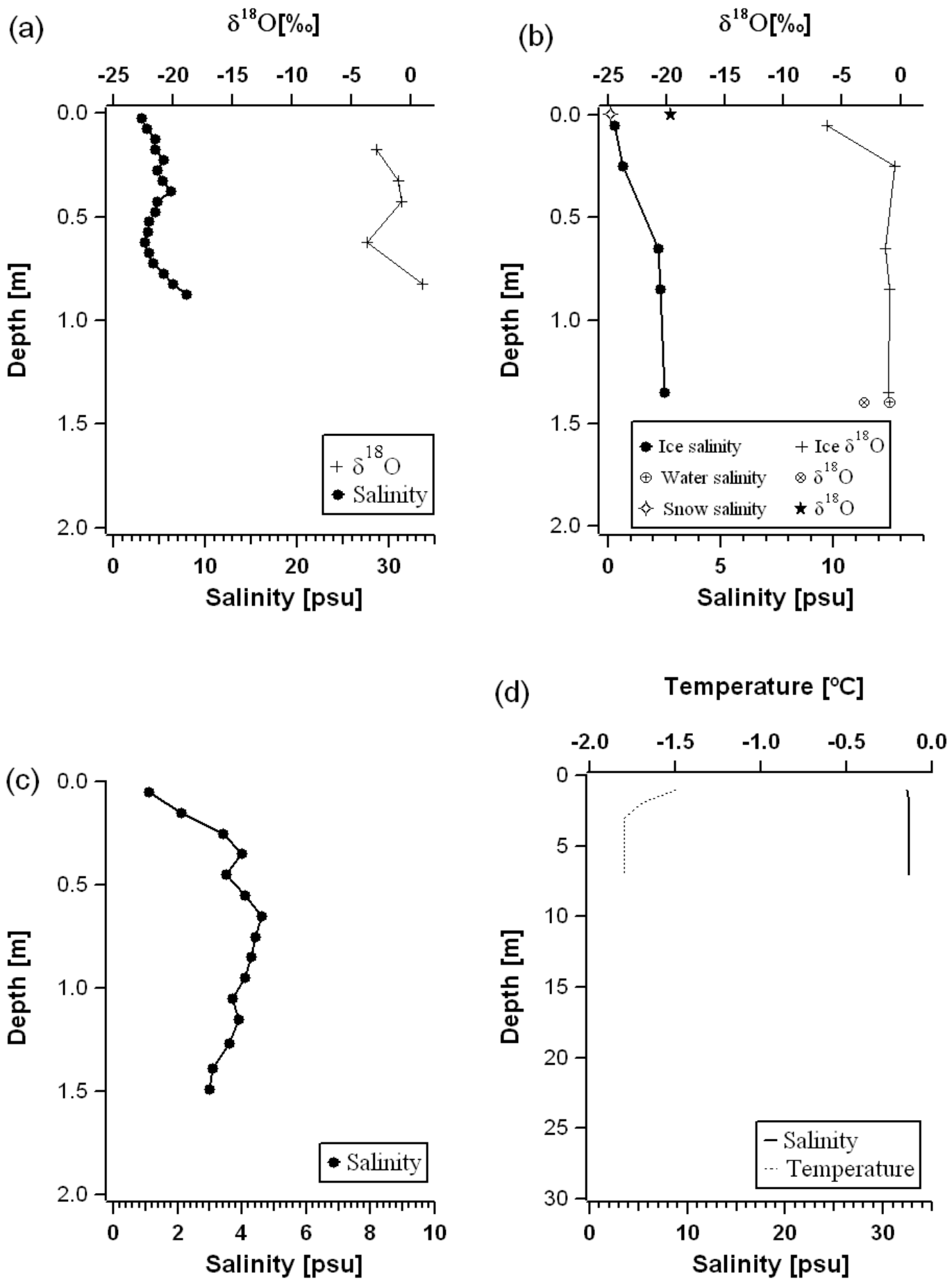
(a)
δ18O[‰]
-25 -20 -15 -10 -5 0
Depth [m]
0.0 0.5 1.0 1.5 2.0
+ δ18O
Salinity
0 10 20 30
Salinity [psu]
(b)
δ18O[‰]
-25 -20 -15 -10 -5 0
Depth [m]
0.0 0.5 1.0 1.5 2.0
Ice salinity
+ Ice δ18O
Water salinity
⊗ δ18O
Snow salinity
★ δ18O
0 5 10
Salinity [psu]
(c)
Depth [m]
0.0 0.5 1.0 1.5 2.0
Salinity
0 2 4 6 8 10
Salinity [psu]
(d)
Temperature [°C]
-2.0 -1.5 -1.0 -0.5 0.0
Depth [m]
0 5 10 15 20 25 30
Salinity
Temperature
0 10 20 30
Salinity [psu]

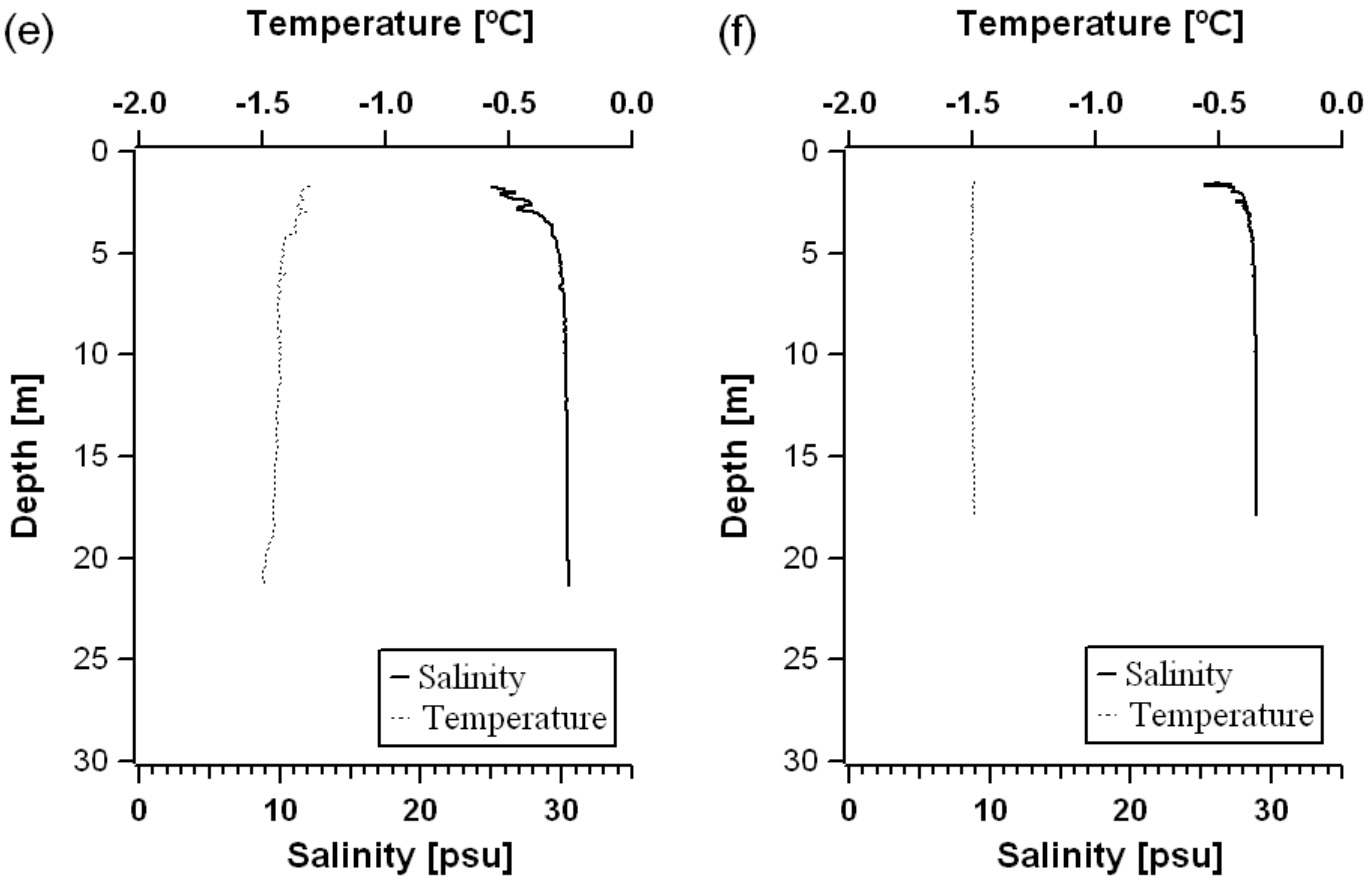


Figure 4. Salinity and $\delta^{18}O$ profile in the ice core, measured (a) at the ice floe (70.67°N, 167.31°W) on 12 May 2002, (b) at the ice floe (78°19'N, 148°2'W) on 22 August 2003, and (c) salinity profile at the ice floe (71°55'N, 154°51'W) on 16 June 2004; and Salinity and temperature profile below the ice, measured (d), (e) and (f) at the corresponding ice floes to (a), (b) and (c), respectively. In (b), ●, +, ⊕, ⊗, ✧ and ★ show values for ice salinity, ice $\delta^{18}O$, water salinity, water $\delta^{18}O$, snow salinity and snow $\delta^{18}O$, respectively.

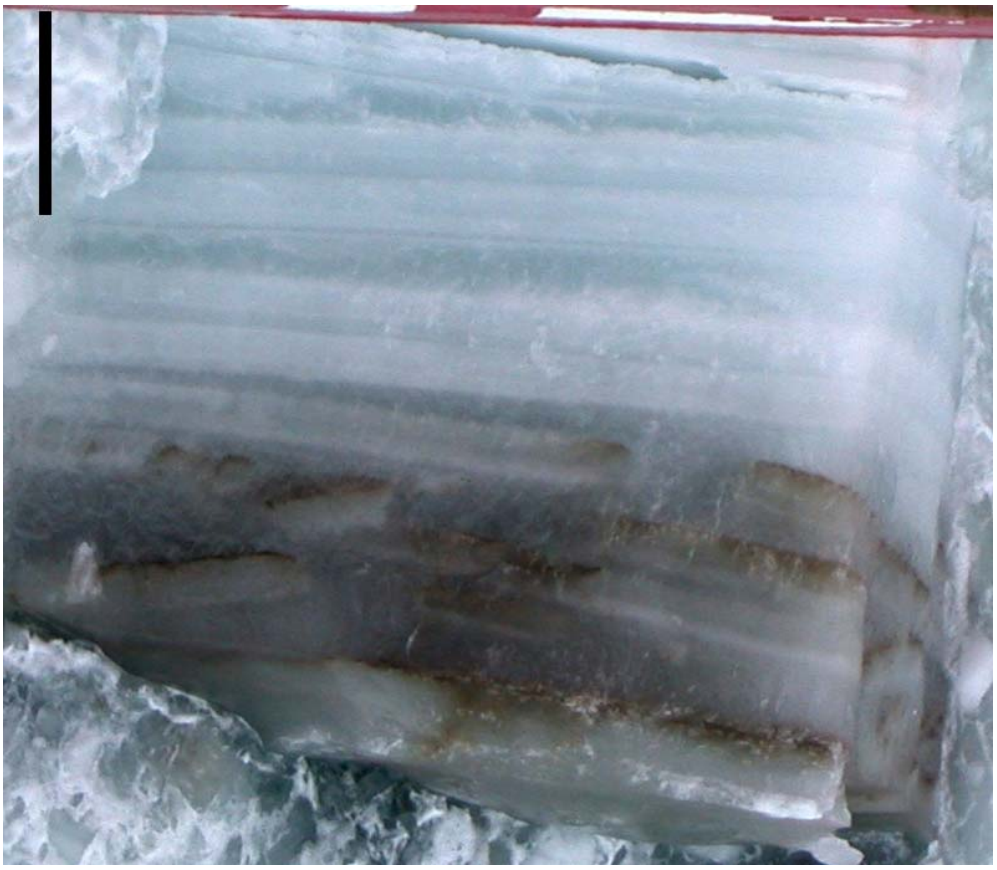

Figure 5. Stratigraphic cross-section of a level ice floe turned on its side along icebreaker hull (top is up, scale bar is 0.5 m). Note the multiple rafts stacked on top one another, with the lower rafts associated with sediment particles entrained into the ice cover during growth.

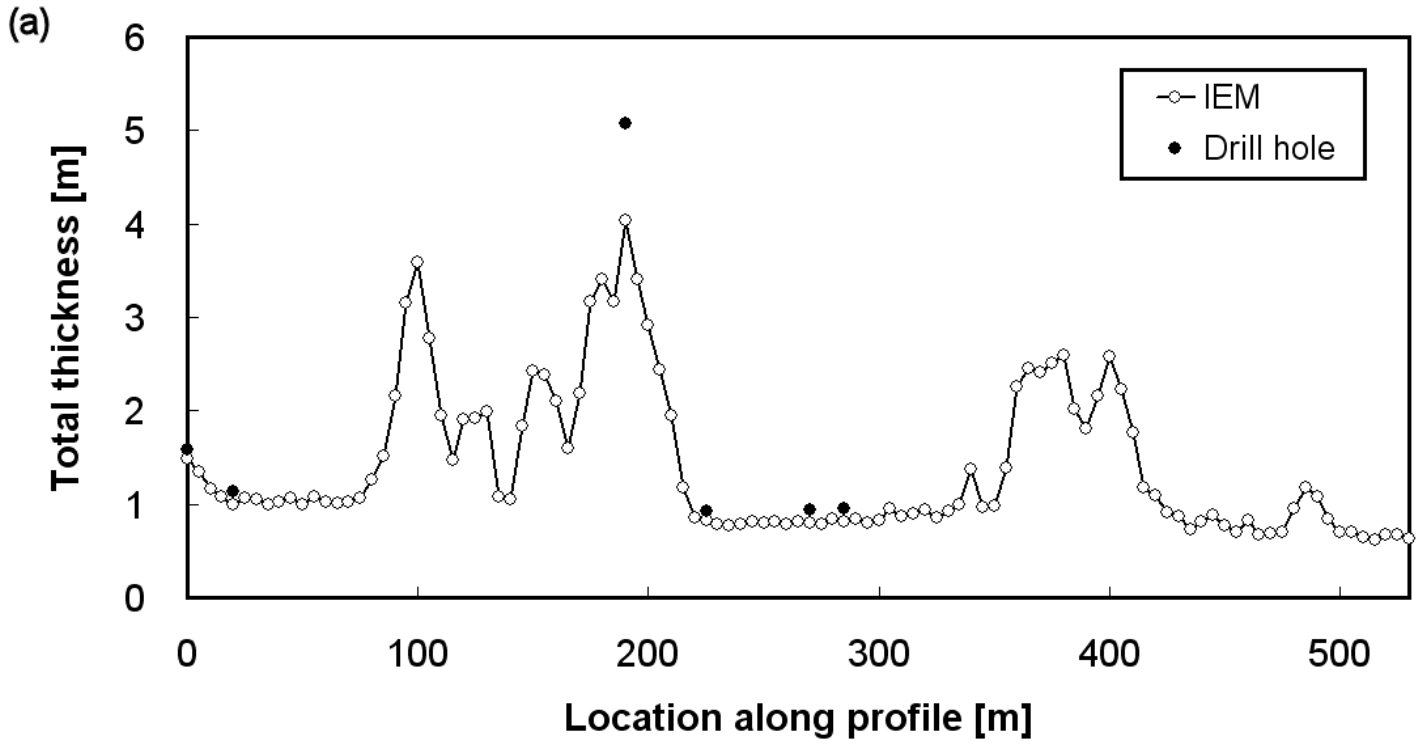


Figure 6. Typical profiles of total thickness (snow depth + ice thickness), measured in (a) 2002, (b) 2003 and (c) 2004 by means of drilling and IEM measurements.

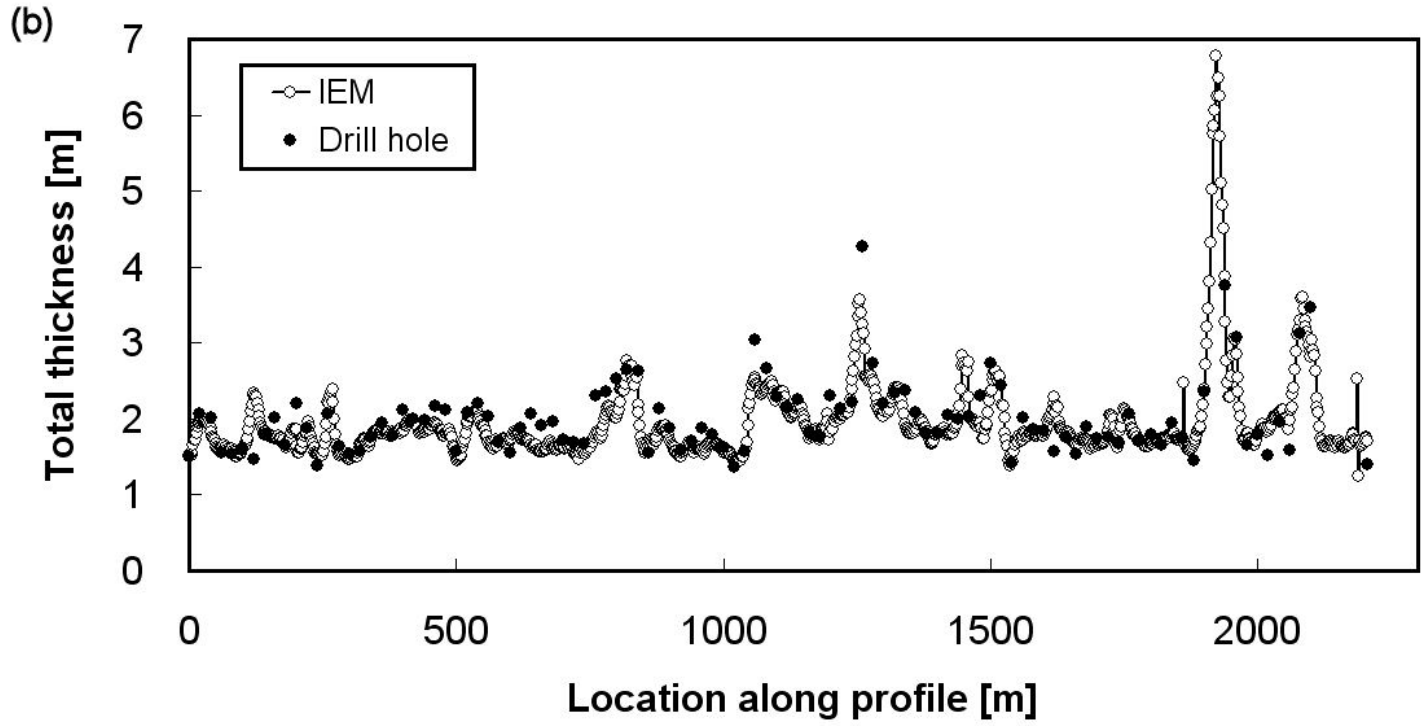


Figure 6. Typical profiles of total thickness (snow depth + ice thickness), measured in (a) 2002, (b) 2003 and (c) 2004 by means of drilling and IEM measurements.

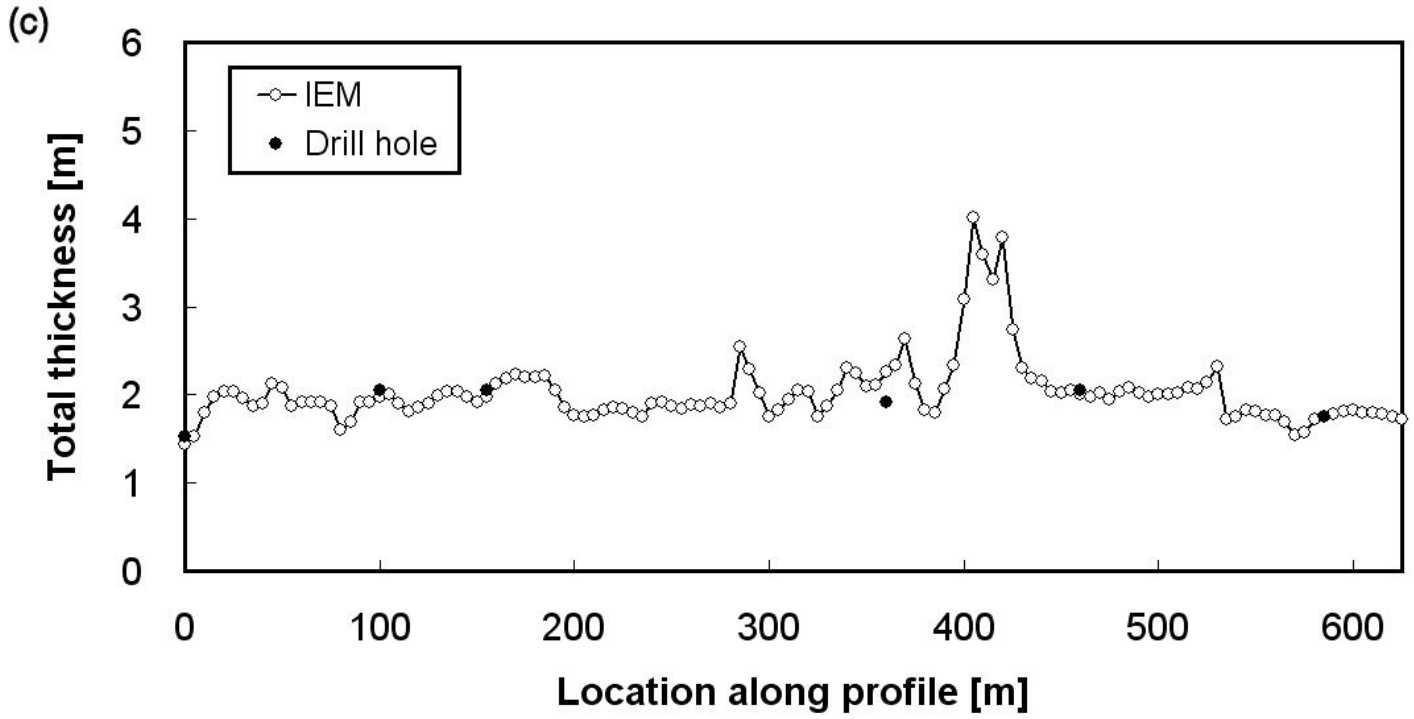


Figure 6. Typical profiles of total thickness (snow depth + ice thickness), measured in (a) 2002, (b) 2003 and (c) 2004 by means of drilling and IEM measurements.

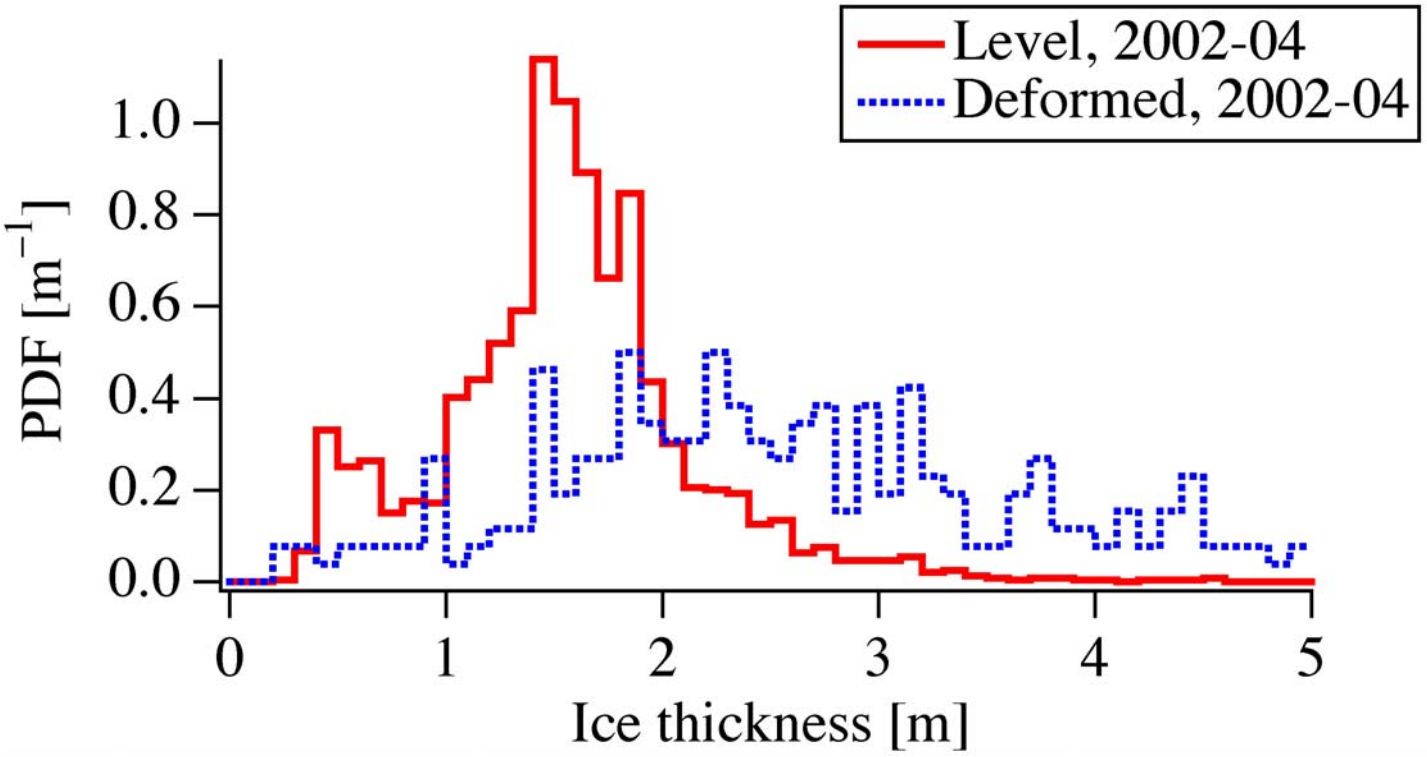


Figure 7. Comparison of ice thickness probability density functions (PDFs) derived for level and deformed ice from IEM measurements in 2002, 2003 and 2004. The bin size is 0.1 m.

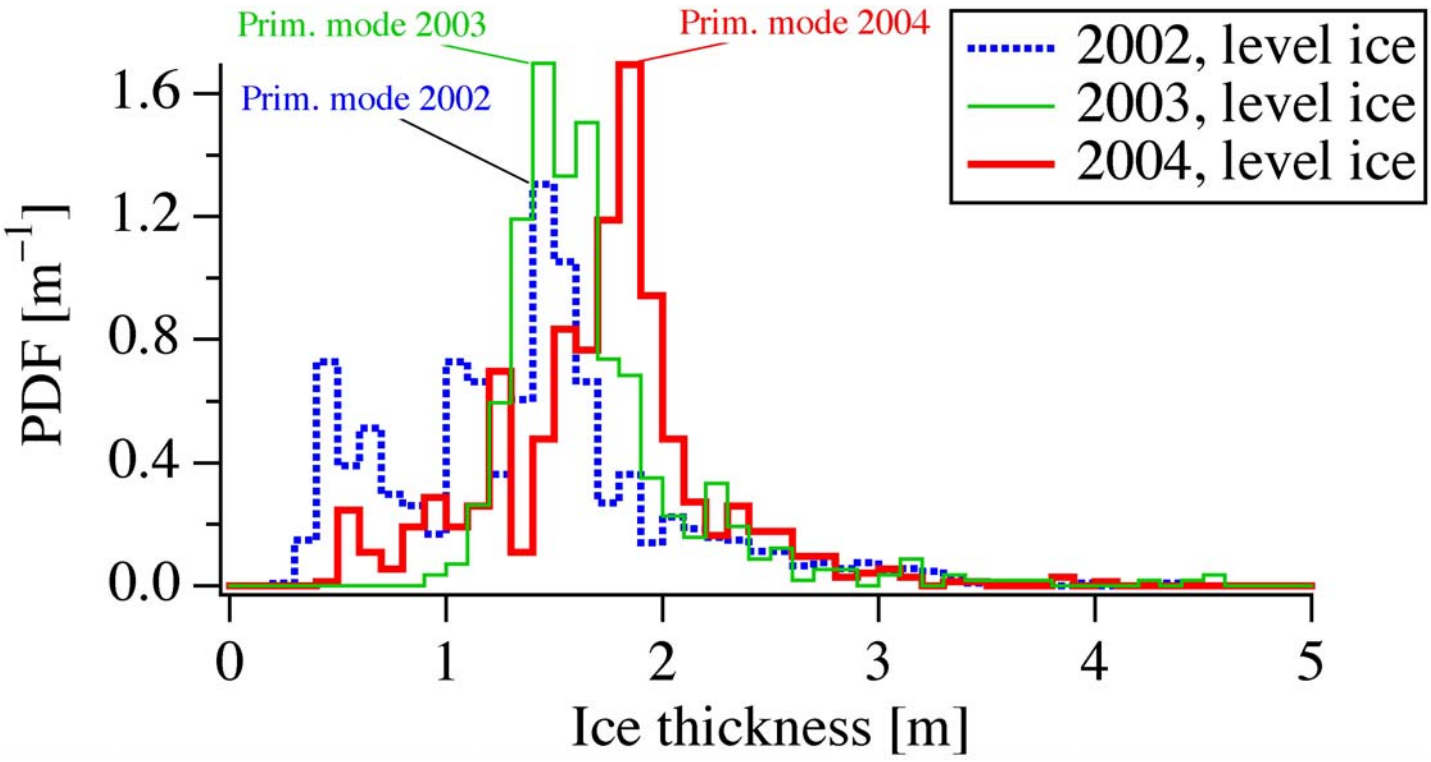


Figure 8. Comparison of ice thickness probability density functions (PDFs) derived from IEM measurements in 2002, 2003 and 2004 for level ice. The bin size is 0.1 m.

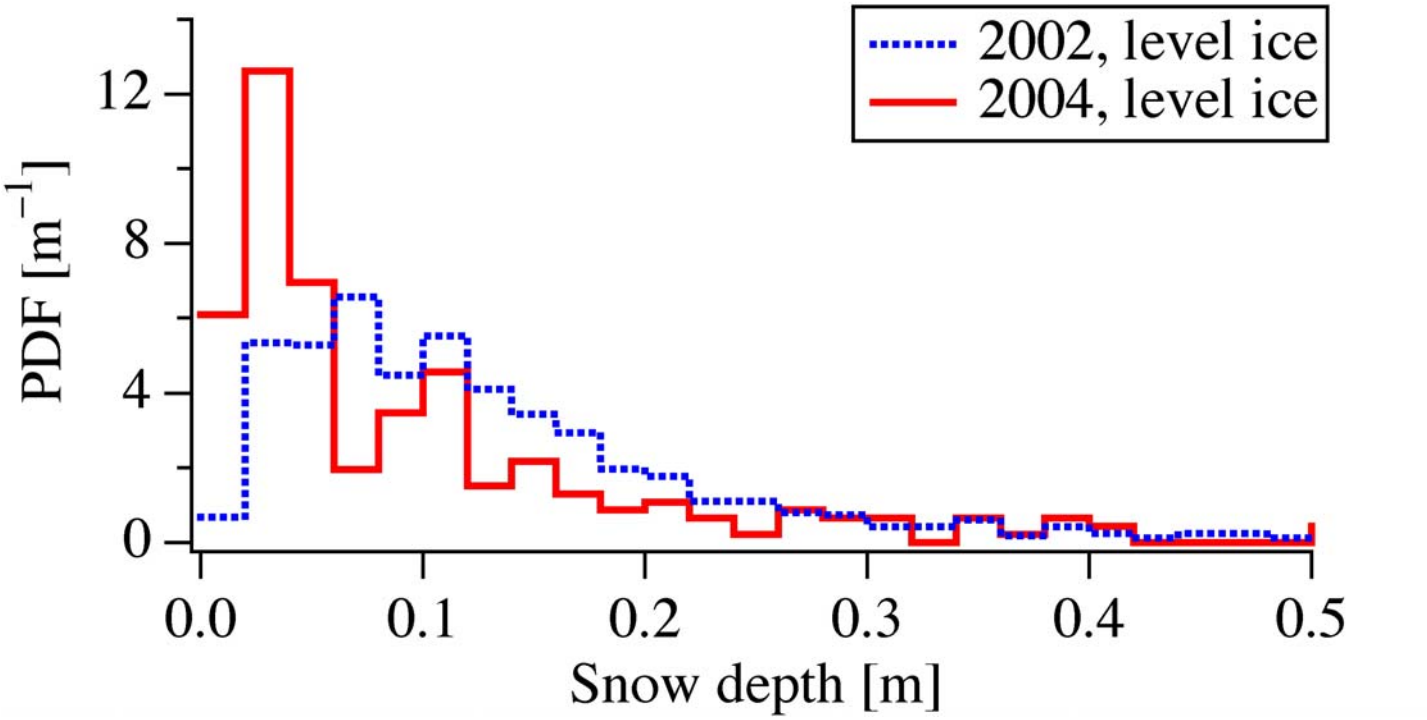


Figure 9. Probability density functions (PDFs) for snow depth on level ice in 2002 and 2004. The bin size is 0.02 m.

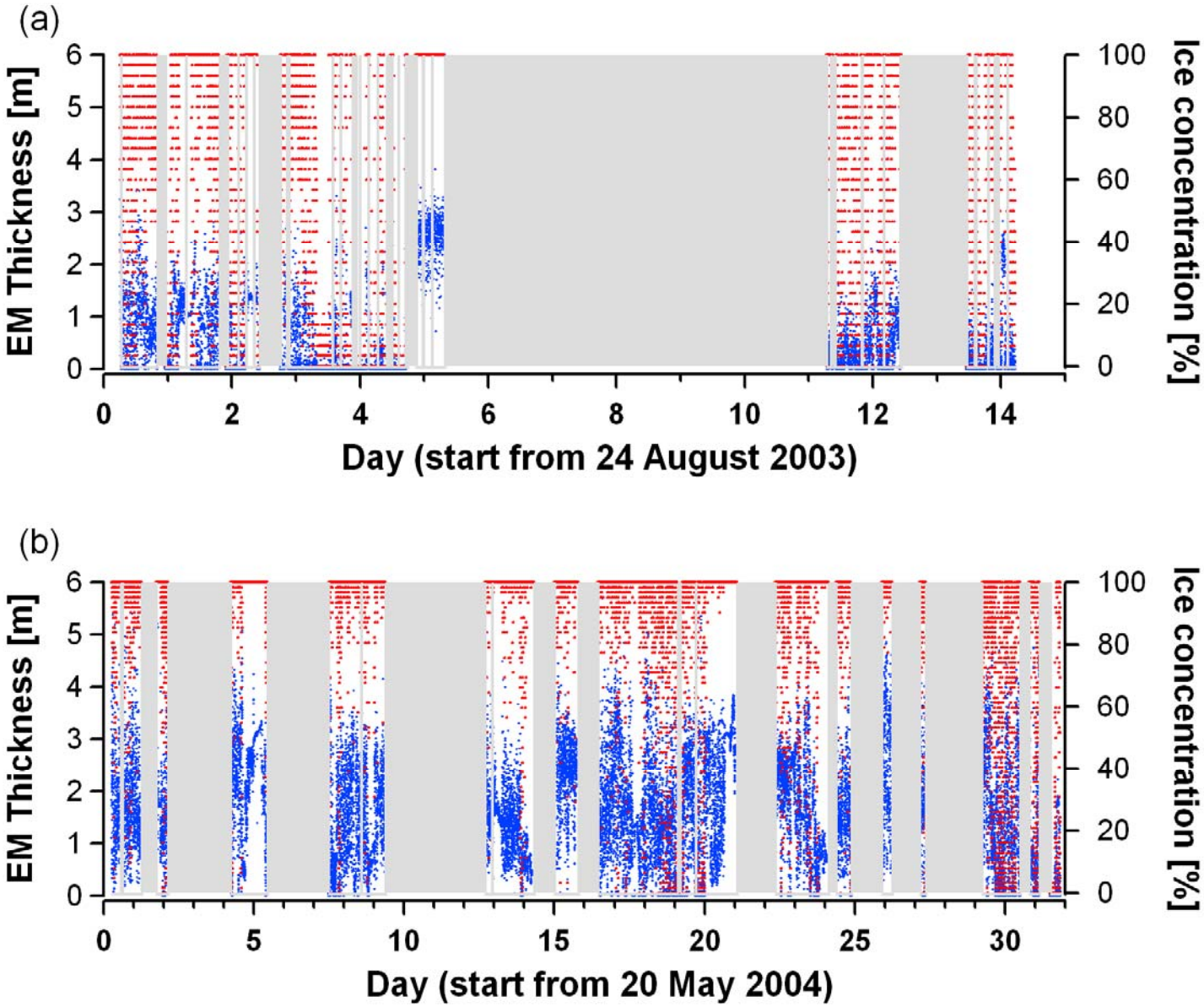


Figure 10. SEM total thickness and ice concentration with time in day (a) starting from 24 August 2003 along the *R/V Xuelong* cruise track, and (b) starting from 20 May 2004 along the *USCGC Healy* cruise track. Ice concentration (in %) was estimated from the open water detected by the laser distance meter at the 1-sec interval over the 1-min measurement period.

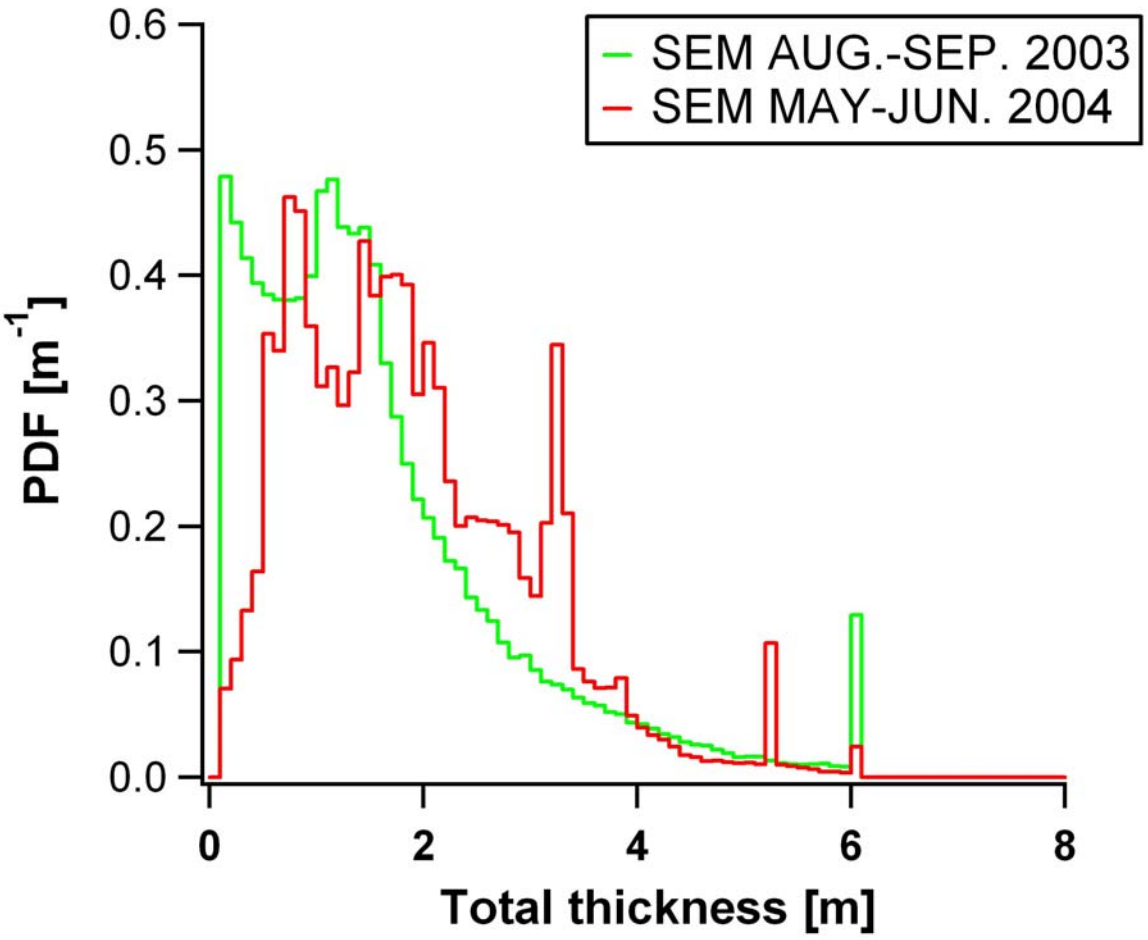


Figure 11. Comparison of total thickness probability density functions (PDFs) derived from SEM measurements in 2003 and 2004. The bin size is 0.1 m.

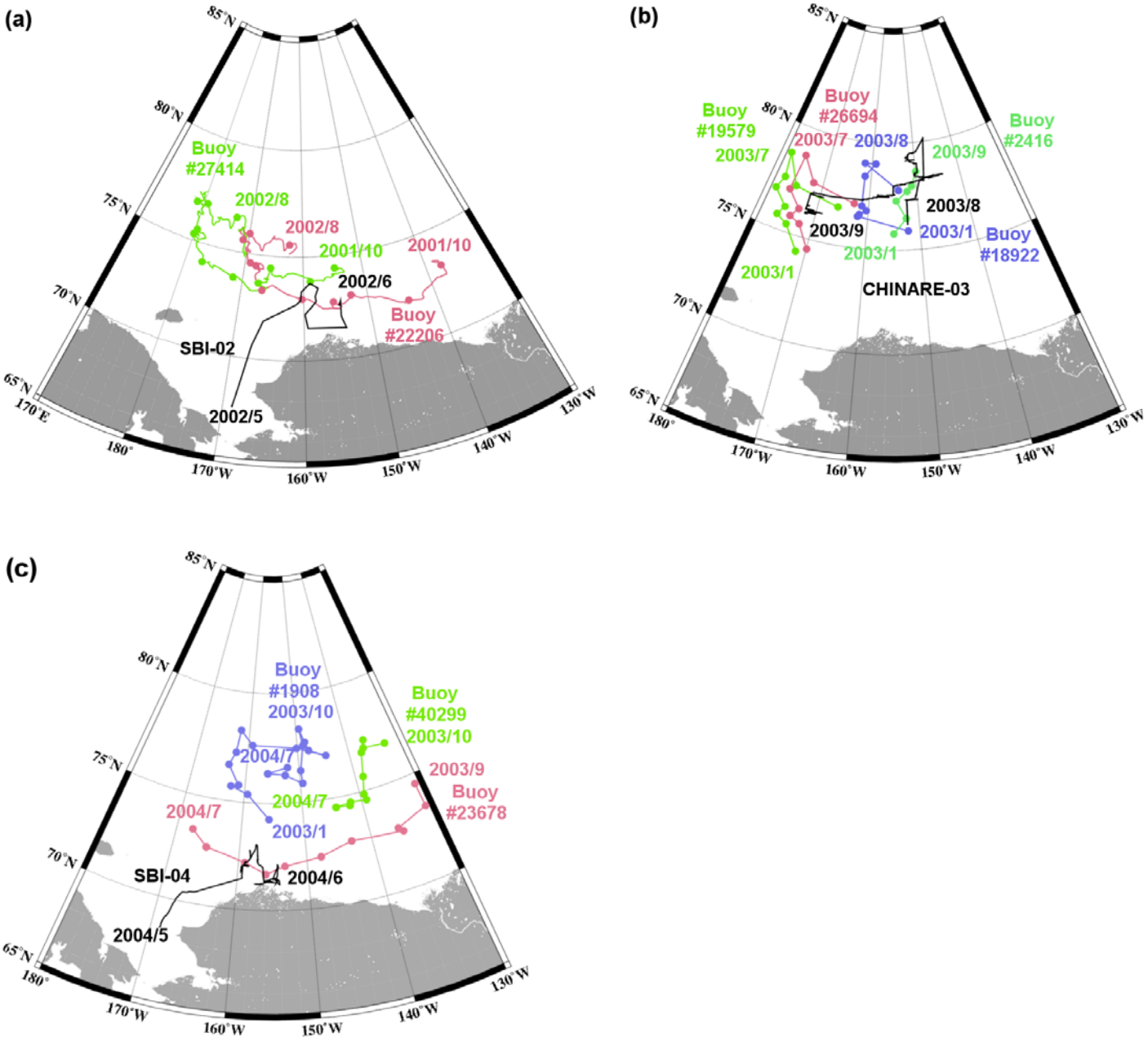


Figure 12. Trajectories of ice drift buoys covering the study area during the period (a) from October 2001 to August 2002, (b) from January 2003 to September 2003, and (c) from January 2003 to July 2004. Data have been obtained from the International Arctic Buoy Program (http://iabp.apl.washington.edu/).

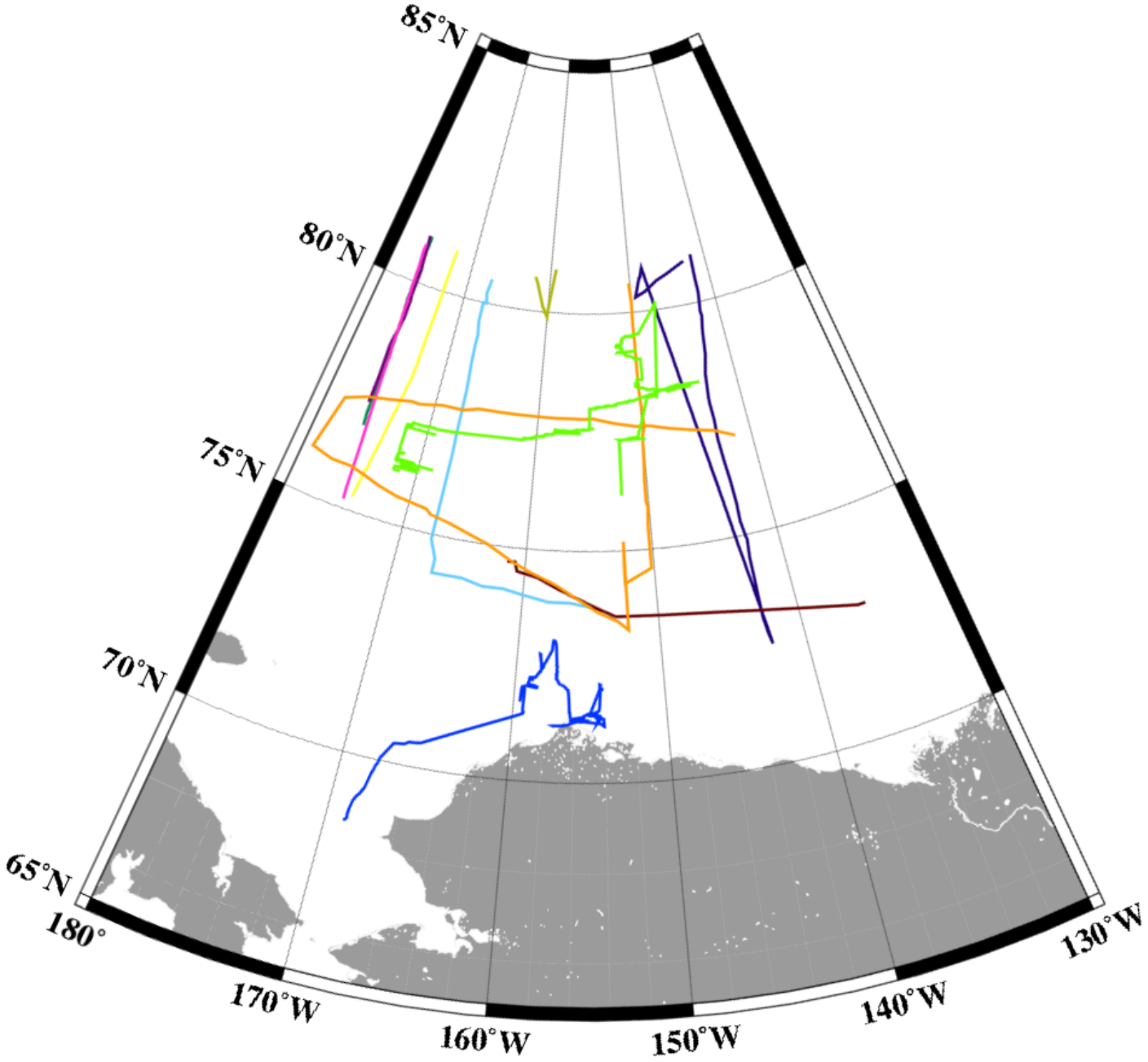


Figure 13. Cruise tracks of submarine sonar measurements of ice draft and SEM total thickness measurements. Shown are tracks by 1986, 1987, 1988, 1989, 1990, 1991, 1992, 1993 and 1994 submarine and by 2003 and 2004 SEM measurements. The colors for each line correspond to those in Fig. 14.

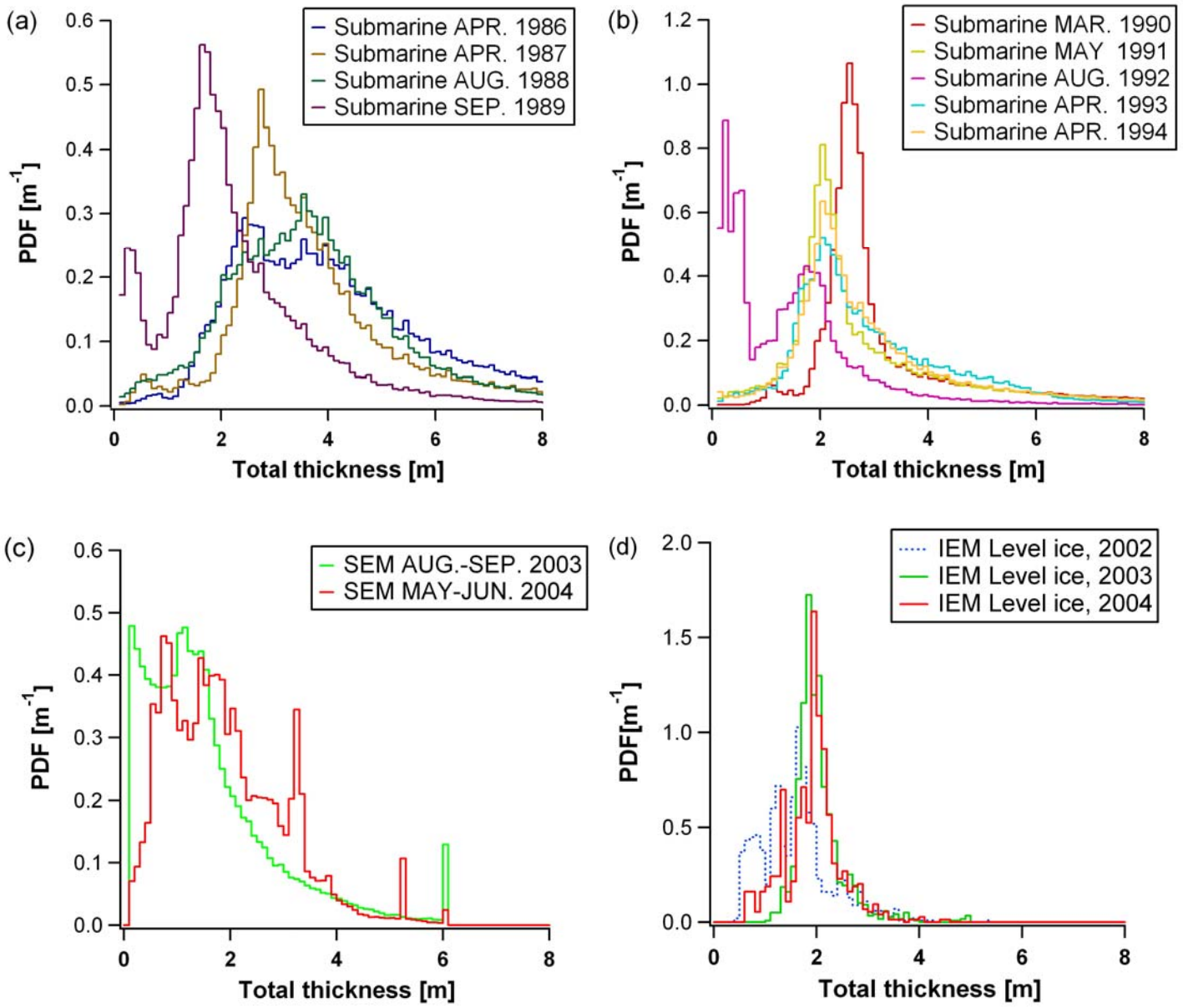


Figure 14. Comparison of total thickness probability density functions (PDFs) derived from submarine sonar measurements of ice draft (converted to ice thickness by multiplying by 1.08 following Wadhams (1998), for spring sea ice of 910 kg $m^{-3}$ density) for (a) 1986, 1987, 1988 and 1989; (b) 1990, 1991, 1992, 1993 and 1994; and (c) SEM measurements in 2003 and 2004; and (d) IEM measurements for level ice in 2002, 2003 and 2004. Submarine sonar data have been obtained from the National Snow and Ice Data Center (2006). The bin size is 0.1 m.

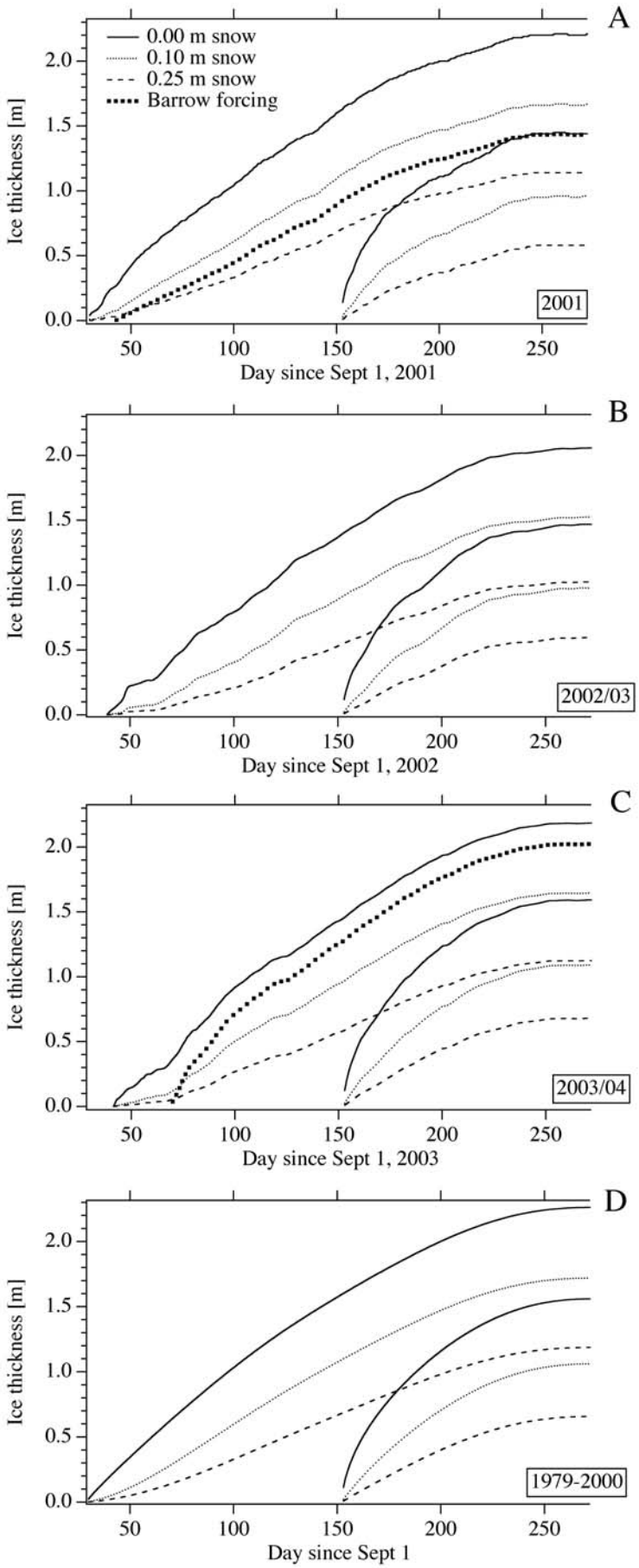


Figure 15: Results of ice-growth simulations with a freezing-degree day model for the ice seasons 2001/02 (A), 2002/03 (B), 2003/04 (C) and climate normals (1979-2000, D). Different curves represent different days of onset of ice formation and different snow depths. Thick, dashed lines indicate conditions as found for Barrow landfast ice in 2001/02 and 2003/04.

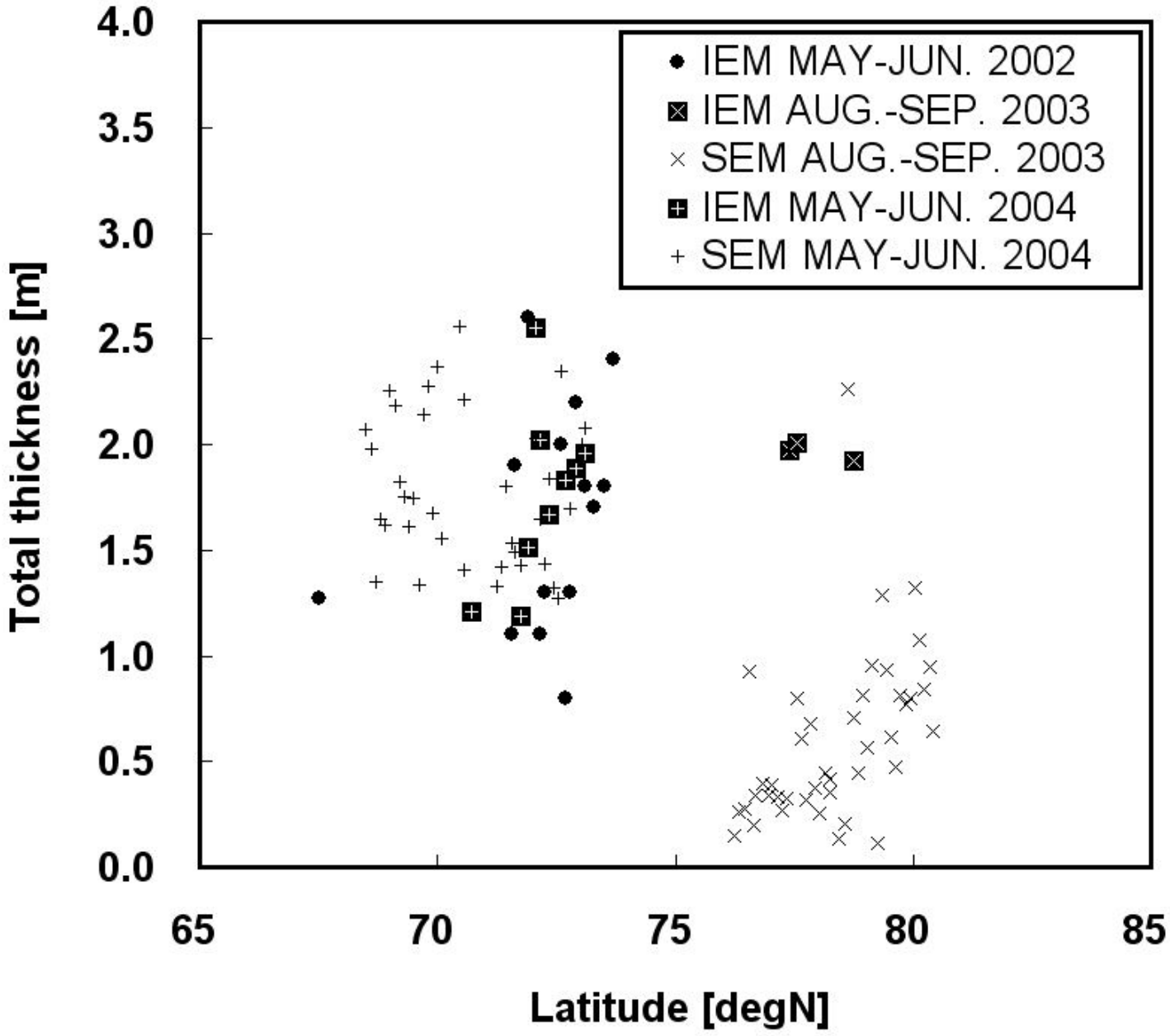


Figure 16. EM-derived total thickness (mean for individual stations or track segments) plotted as a function of latitude.

Sea-ice thickness variability in the Chukchi Sea, spring and summer 2002-2004
Shirasawa et al.